Review

Laser Manufacturing of Superwetting Oil–Water Separation Materials: A Review

Wei Xiong [1,†], Linfeng Zhu [1,†], Ruisong Jiang [1,*] and Chaolang Chen [1,2,*]

[1] School of Mechanical Engineering, Sichuan University, Chengdu 610065, China; weixiong202309@163.com (W.X.); linfengzhu2021@163.com (L.Z.)
[2] National United Engineering Laboratory for Advanced Bearing Tribology, Henan University of Science and Technology, Luoyang 471023, China
[*] Correspondence: jiangrs@scu.edu.cn (R.J.); chaolangchen@scu.edu.cn (C.C.)
[†] These authors contributed equally to this work.

Abstract: The frequent occurrence of oil spills and the massive discharge of oily wastewater pose a significant threat to sustainable and healthy human development. Therefore, it is of importance to effectively separate oil–water mixtures. Inspired by nature, many superwetting surfaces/materials for oil–water separation have been developed in recent years. However, these surfaces/materials are subject to certain limitations and are unable to fully meet practical needs. With the advancement of laser technology, a novel solution has been provided for fabricating superwetting oil–water separation materials. Based on the design theory and separation mechanism, this paper summarizes the research progress of the laser-fabricated superwetting surfaces/materials for oil–water separation in recent years. First, the basic wetting theory, design strategy, and oil–water separation mechanism of the laser-fabricated materials are introduced in detail. Subsequently, the laser-fabricated oil–water separation materials, including superoleophilic/superhydrophobic materials, superhydrophilic/superoleophobic materials, and materials with reversible or superamphiphilic wettability, are systematically summarized and analyzed. Finally, the challenges and future research directions of laser-fabricated superwetting oil–water separation materials are discussed.

Keywords: laser manufacturing; wettability; oil–water separation; superhydrophobic; superhydrophilic

1. Introduction

Fossil fuels are an essential source of energy for the sustenance of humanity in modern societies. Particularly since the twentieth century, the extensive exploitation of petroleum resources commenced as a result of the Industrial Revolution. With the rapid development of the economy and society, the demand for oil has correspondingly increased, posing a significant threat to the global ecological environment and human health due to the substantial occurrence of oil spills [1–6]. For example, approximately 10.8 million barrels of crude oil were discharged into the water body of the Gulf during the Gulf War in 1991 [7–10]. In 2010, a major oil spill lasted for three months, with thousands of barrels of oil discharged daily, known as the BP Oil Spill [11–14]. Furthermore, the constant discharge of oily industrial wastewater has inflicted irreparable damage upon the soil and water environment [15–19]. However, traditional oil–water separation methods [20], such as gravity separation [21], chemical decomposition [22], and centrifugation [23,24], while capable of separating most of the oil in the water, still present challenges, including high energy consumption, low filtration, and secondary pollution to the environment. Hence, there is an urgent need to seek a new generation of oil–water separation solutions.

Inspired by nature, the use of superwetting materials for separating oil–water mixtures has garnered extensive attention [25–48]. Superwetting materials, including superhydrophobic/superoleophilic and superhydrophilic/superoleophobic materials, can be

fabricated by modifying the microstructures and chemical energy of the surface. These materials exhibit opposite wetting behaviors towards oil and water, making them suitable for oil–water separation applications [4,26,49–54]. In general, strategies for separating stratified oil–water mixtures using superwetting materials can be divided into three groups: (1) removing water from oil–water mixtures; (2) removing oil from oil–water mixtures; and (3) selectively removing oil or water from oil–water mixtures. Compared to traditional oil–water separation materials, superwetting materials offer notable advantages, including high separation efficiency and flux, good selectivity, and self-cleaning properties [55]. For example, conventional membranes tend to suffer from pore plugging and surface-coating damage due to the accumulation of oil pollutants over repeated use, resulting in decreased separation efficiency and oil–water flux. In contrast, for superhydrophilic/superoleophobic membranes, these issues could be avoided [56]. However, existing superwetting materials still have certain limitations, such as complex manufacturing processes, stringent requirements on materials, and high maintenance costs. Furthermore, the surface micro–nano structures and the size and porosity of the pores greatly impact the separation performance of superwetting materials in terms of efficiency, flux, and durability. Therefore, achieving the precise fabrication of surface micro–nano structures and pore structures of the superwetting materials is crucial for promoting their practical applications in industry [26,52,54,57–60].

In recent years, ultrafast lasers, including nanosecond, picosecond, and femtosecond lasers, have been widely used to fabricate superwetting materials for separating oil–water mixtures [61]. A diverse range of materials, such as metals, alloys, polymers, and even biomaterials, are well-suited for laser processing. The technology of ultrafast laser processing offers high machining accuracy, small heat-affected zone, and strong versatility, enabling the construction of various surface morphologies with different characteristics. On the one hand, the surface is roughened by the micro–nano structures created by laser ablation, and its hydrophilicity is enhanced according to the Wenzel model. On the other hand, when the roughened surface is hydrophobically modified, the air is trapped in the laser-fabricated micro–nano structures, resulting in a reduced solid–liquid contact area and preventing water from wetting based on the Cassie–Baxter model. In addition, surface wettability can be effectively controlled by adjusting the processing parameters, such as laser power, scanning speed, and scanning spacing. Consequently, ultrafast laser processing significantly contributes to the strong selectivity of the superwetting materials towards oil and water.

In this paper, the laser-manufactured superwetting materials for oil–water separation are comprehensively reviewed. First, the significance of environmentally friendly and efficient oil–water separation technology is highlighted in the face of the global threat of oil pollution. Second, based on the analysis of the theoretical basis of wettability, the design strategy and oil–water separation mechanism of the laser-fabricated superwetting materials are introduced. Subsequently, according to the different substances separated from the mixtures, various ultrafast laser-processing methods for fabricating oil–water separation materials and the separation performances of these fabrications are reviewed and discussed in depth. Finally, the current limitations of ultrafast laser processing are addressed and the prospects for realizing efficient and multi-purpose oil–water separation through laser-processed materials are discussed.

2. Wettability Theory and Design Strategy of Laser-Fabricated Oil–Water Separation Materials

2.1. Basic Wettability Theory

Wettability refers to the ability of a liquid to spread over a solid surface, serving as the theoretical basis of superwetting materials for oil–water separation. In 1850, the theory of surface wettability was first proposed by Young [62,63]. The wettability of a solid surface is

typically quantitatively assessed by the contact angle (CA) θ and the sliding angle (SA) α. Young's equation can be expressed as Equation (1):

$$\cos\theta = \frac{\gamma_{SA} - \gamma_{SL}}{\gamma_{LA}} \tag{1}$$

where θ is the CA on an ideal smooth surface, γ_{SA} and γ_{SL} are the interfacial energy/tension of the solid–air and solid–liquid, respectively, and γ_{LA} denotes the interface energy/tension between liquid and air [46,64] (Figure 1a). The SA is the angle between the inclined plane and the horizontal plane when the surface is gradually tilted to the point where the droplet is just able to slide [65] (Figure 1b).
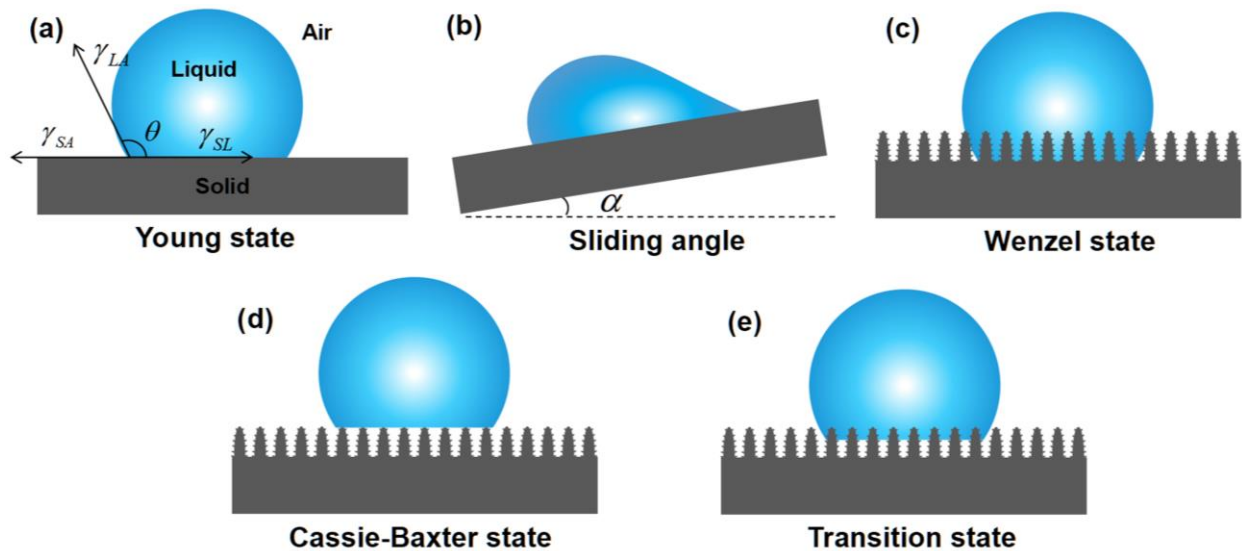

Figure 1. Diagrams of water wetting states: (**a**) Young state, (**b**) Sliding angle model, (**c**) Wenzel state, (**d**) Cassie–Baxter state, and (**e**) Transition state.

The ideal smooth surface described by Young does not exist in real life. Inspired by Young's theory of wettability, Wenzel introduced the concept of surface roughness [63,66] (Figure 1c), and the modified equation is as follows:

$$\cos\theta_L = R\cos\theta \tag{2}$$

where θ_L is the CA on the rough surface, and R denotes the surface roughness.

The Wenzel state describes a liquid fully wetting a solid surface, while there is another case in nature where the liquid cannot thoroughly wet the solid surface. In this scenario, the liquid contacts the air in the microstructures (Figure 1d), and the Cassie–Baxter equation is derived as follows [45,67]

$$\cos\theta_L = f\cos\theta + f - 1 \tag{3}$$

where f is the area fraction of the liquid in contact with the solid surface.

However, when subjected to external pressure, the liquid is forced into microgrooves on the microscopic surfaces of solids. In this case, the Cassie model no longer applies and can be replaced by a transitional form of the Transition state (Figure 1e).

Based on the analysis of the background theories of wettability, it can be concluded that a water droplet in contact with a solid surface in the air has four wetting states. When the water contact angle (WCA) is >90°, it indicates the solid surface is hydrophobic. When the WCA is >150° and the SA < 10°, the solid surface is superhydrophobic. In this case, the water droplets can easily slide off the solid surface. When the WCA is <90°, the solid surface is hydrophilic. When the WCA is < 10°, the solid surface is superhydrophilic. In this case, the water droplets can hardly fall off the solid surface as a result of the strong

adsorption of water on the surface. Correspondingly, there are also four states of an oil droplet contacting a solid surface.

2.2. Wettability Theory of Underwater Oil

Similar to a droplet in contact with a solid surface in the air, wetting occurs when oil comes into contact with solid underwater surfaces. Therefore, the Young, Wenzel, and Cassie–Baxter states can also be used to describe the wetting behaviors of an underwater oil droplet on solid surfaces (Figure 2).
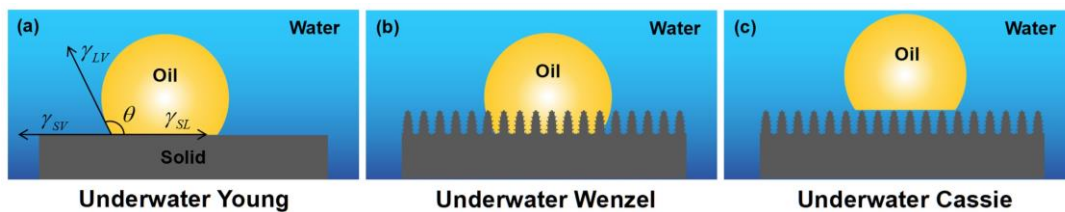

Figure 2. Diagrams of underwater oil wettability states: (**a**) underwater Young state, (**b**) underwater Wenzel state, and (**c**) underwater Cassie state.

When an oil droplet contacts an ideal smooth surface underwater, Young's equation can be expressed as [39,65,68]:

$$\cos\theta_{OW} = \frac{\gamma_{OA}\cos\theta_O - \gamma_{WA}\cos\theta_W}{\gamma_{OW}} \tag{4}$$

where θ_{OW} is the underwater contact angle of oil on a smooth surface; θ_O and θ_W denote the Young's contact angles of oil droplets and water droplets in the air, respectively. γ_{OA}, γ_{WA}, and γ_{OW} refer to the surface tension at the oil–air, water–air, and oil–water interfaces, respectively.

Because the surface tension of water is much greater than that of oil ($\gamma_{OA} << \gamma_{WA}$), the contact angle is $\theta_O < \theta_W$. It can be deduced from Equation (4) that hydrophilic materials typically exhibit oleophobicity underwater. Similar to the Wenzel and Cassie states in air, the impact of surface roughness on the wettability of an underwater oil droplet on a rough solid surface can be described by the underwater Wenzel state and underwater Cassie state as [69]:

$$\cos\theta^W_{OW} = R\cos\theta_{OW} \tag{5}$$

$$\cos\theta^C_{OW} = f\cos\theta_{OW} + f - 1 \tag{6}$$

where θ_{OW}, θ^W_{OW}, and θ^C_{OW} denote the underwater contact angle of the oil in states that are underwater Young, underwater Wenzel, and underwater Cassie, respectively. R denotes the surface roughness, and f is the area fraction of underwater oil in contact with the solid surface.

2.3. Oil–Water Separation Mechanism of Superwetting Materials

The liquid intrusion pressure (ΔP) refers to the minimum pressure at which the liquid on the surface of the material initiates intrusion into the pores under external pressure, and it is an important physical quantity affecting the oil–water separation performance. This pressure can be calculated by the Laplace equation [70]:

$$\Delta P = \frac{2\gamma}{R} = -\frac{l\gamma\cos\theta}{A} \tag{7}$$

where γ is the surface tension of the liquid; R, l and A are the radius, perimeter, and cross-sectional area of the pore, respectively; θ is the contact angle of the droplet. For super-oleophilic/superhydrophobic oil–water separation materials, the contact angle of oil (θ_o) is <10° and the contact angle of water (θ_w) is >150°, resulting in the intrusion pressure of oil

being (ΔP_{o}) < 0 and the intrusion pressure of water being (ΔP_{w}) > 0 (Figure 3a,b). Therefore, when heavy oil–water mixtures come into contact with superoleophilic/superhydrophobic surfaces, the heavy oil can easily pass through the surfaces, while the water cannot. For superhydrophilic/superoleophobic oil–water separation materials, the contact angle of water (θ_{w}) is <10° and the underwater contact angle of oil (θ_{o}) is >150°, resulting in the intrusion pressure of water being (ΔP_{w}) < 0 and the intrusion pressure of underwater oil being (ΔP_{o}) > 0 (Figure 3c,d). Therefore, when light oil–water mixtures come into contact with the superhydrophilic/superoleophobic surfaces, the water can freely pass through the surfaces quickly, while the light oil is fully blocked.
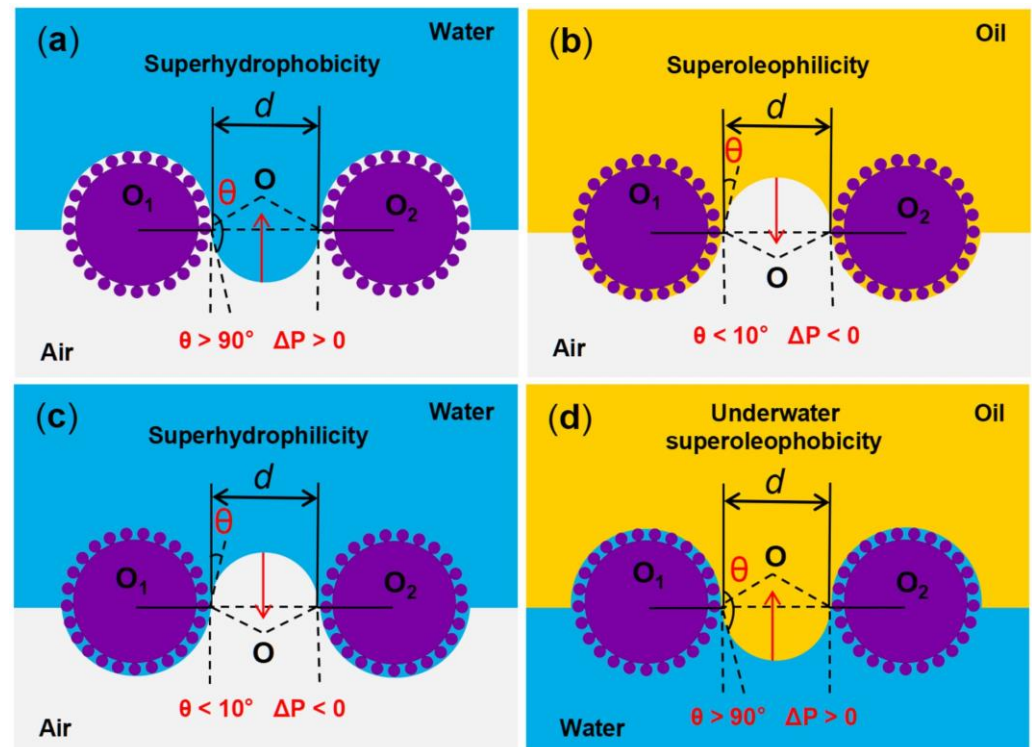

Figure 3. Schematic diagram of the oil–water separation mechanism of superwetting porous materials. (**a**,**b**) Oil can pass through the superoleophilic/superhydrophobic surfaces, while water cannot. (**c**,**d**) Water can pass through the superhydrophilic/superoleophobic surfaces, while oil cannot.

2.4. Design Strategy of Laser-Fabricated Oil–Water Separation Materials

Ultrafast laser processing is acknowledged for its non-contact nature, having high processing quality and precision. In comparison to other processing methods, ultrafast laser processing offers unique advantages due to the little collateral damage caused by the shock waves and heat conduction generated in the material being processed [71–75]. Under ultrafast laser irradiation, ablation or melting occurs when the lattice temperature of the substrate rises to a specific value (the temperature depends on the electron–phonon coupling strength of the material). Ablation, as the primary action mode of laser processing, occurs in several ways, such as evaporation [76], spallation [77,78], phase explosion [79,80], and fragmentation [81]. The micro–nano structures on the surface are formed after the ablation area cools down and re-solidifies [72].

A typical ultrafast laser-processing system is illustrated in Figure 4a. The laser beam emitted from the laser generator is attenuated by an attenuator to produce a beam with a specified power. It is then incident into a scanning galvanometer after being expanded and finally focused on the sample surface after being reflected by several mirrors and a dichroic mirror. Simultaneously, the illumination beam is transmitted through the dichroic mirror and incident into the CCD camera. The movement of the processing platform in three

dimensions (3D) and the ultrafast laser-processing parameters are precisely controlled by a computer [75,82].

In recent years, ultrafast laser micro–nano processing has been extensively applied in modifying the surface wettability of solid materials [61]. A variety of complex micro–nano structures can be precisely manufactured on different material surfaces by ultrafast laser-processing technology [83–96]. For instance, Yang et al. [97] systematically studied the mechanism of the wettability transition on nanosecond laser-ablated aluminum substrate surfaces. The ablated aluminum surfaces formed micro-/nanoscale rough structures with a large number of protrusions and overlying particles (Figure 4b). These multilayered surface structures with large air pockets greatly reduced the contact area between the actual surface and the droplets. As the laser-abraded rough surfaces absorbed organic matter in the air, the wettability of the surface gradually transformed from superhydrophilicity to superhydrophobicity after exposure to ambient air for a month.

Ultrafast laser processing not only effectively controls the wettability of materials by producing micro–nano structures, but it also adjusts the pore structures (e.g., pore size and porosity) of the materials on demand. Wang et al. [98] prepared microholes arrayed on titanium foil with controllable wettability by a femtosecond laser. The laser-treated microholes exhibited varying sizes at different processing parameters, and their diameters increased with the rise in pulse number and pulse energy within a certain range (Figure 4c). Furthermore, the surface superhydrophilicity and superhydrophobicity of the as-prepared Ti foil could be repeatedly converted by high-temperature treatment in a dark room and immersion in alcohol under UV irradiation.

In addition, the laser-induced periodical surface structures (LIPSS), which are micro- and nanoscale rough structures formed by laser irradiation, can significantly change the surface morphology and chemical composition of the material, thus altering its surface energy and roughness [99–103]. For instance, Gaudiuso et al. [104] used sub-THz bursts of femtosecond laser pulses to prepare surface-textured copper with superhydrophobic properties. Under specific laser-irradiation conditions, the as-prepared copper surfaces formed double-scale hierarchical texture structures, constituted by LIPSS and random nanoparticle decoration (Figure 4d). These special structures endowed the copper surface with superhydrophobic and anti-adhesion properties. Martínez-Calderon et al. [105] prepared highly hydrophobic stainless-steel surfaces with dual-scale rough structures by a femtosecond laser (Figure 4e). These rough structures consist of the micro-pattern and the LIPSS nano-pattern, resulting in a static contact angle of the stainless-steel surface higher than 150°.

Figure 5 summarizes the design strategy of laser-fabricated superwetting porous materials for oil–water separation. Generally, the hydrophobic materials are transformed from hydrophobic/oleophilic to superhydrophobic/superoleophilic by laser-fabricating mico–nano structures on the surface, thus realizing water-blocking oil–water separation. In addition, the pores required for oil passage can also be fabricated by ultrafast lasers. Similarly, the superhydrophilic/underwater superoleophobic porous materials for oil-blocking oil–water separation can be fabricated from hydrophilic materials based on ultrafast laser processing.
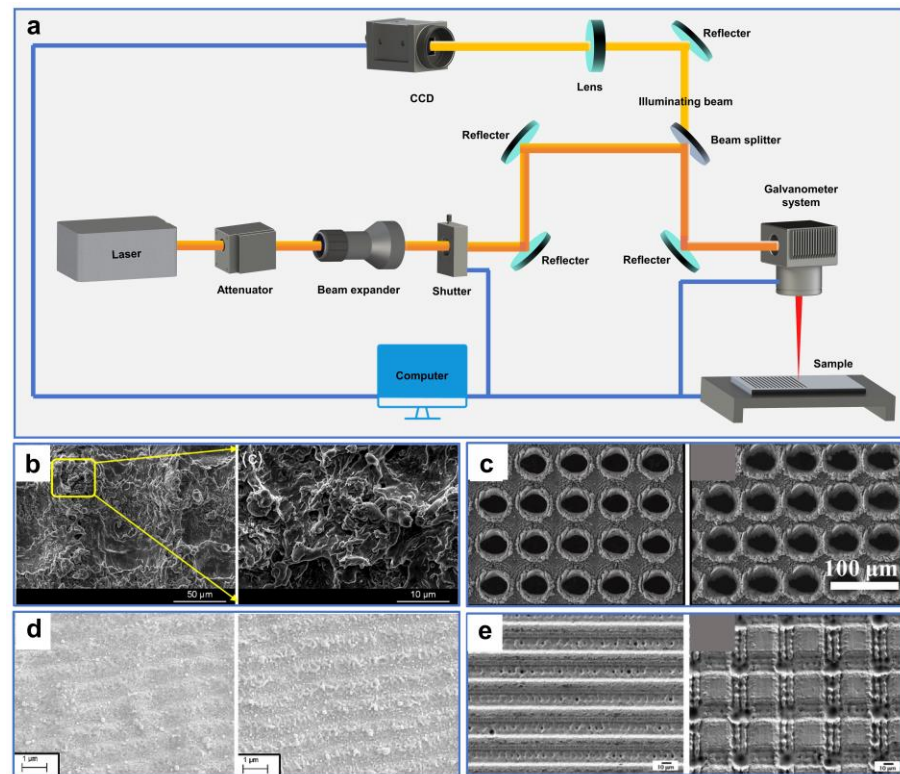
Figure 4. (**a**) Schematic diagram of a typical ultrafast laser-processing system. (**b**) SEM images of laser-ablated aluminum surfaces. Reproduced from ref. [97] with permission from Elsevier (copyright 2018). (**c**) SEM images of fabricated samples by different femtosecond laser energy and pulse number. Reproduced from ref. [98] with permission from Chinese Optics Letters (copyright 2021). (**d**) SEM images of fabricated copper surfaces with double-scale hierarchical texture structures by different laser parameters. Reproduced from ref. [104] with permission from Elsevier (copyright 2023) (**e**) SEM images of the fabricated hierarchical structures on stainless steel surfaces. Reproduced from ref. [105] with permission from Elsevier (copyright 2016).
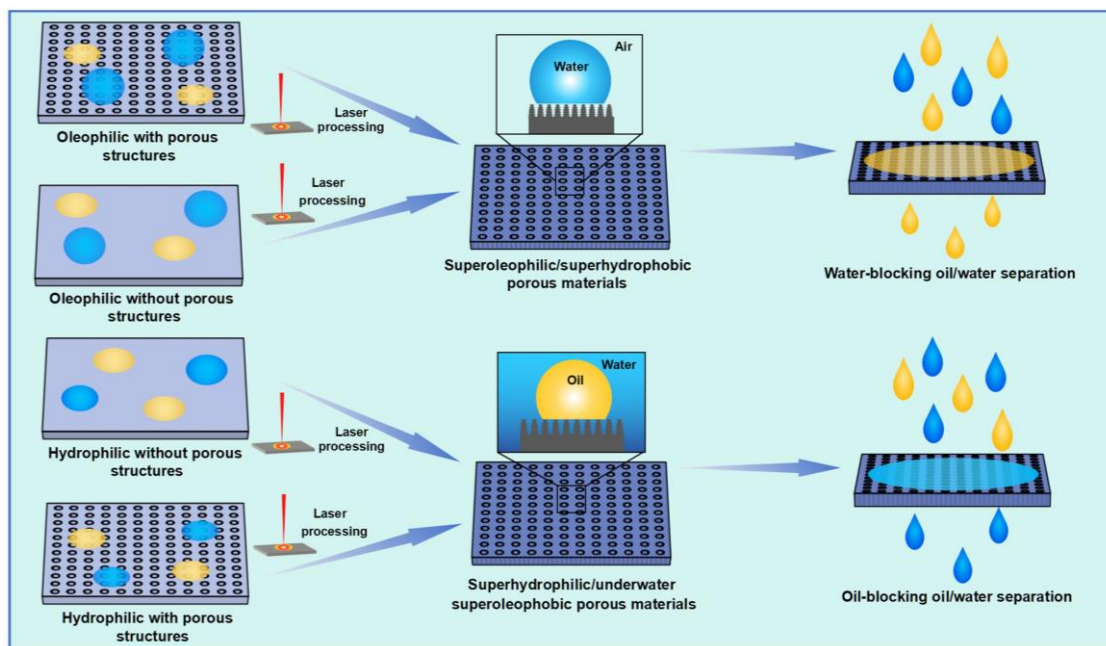

Figure 5. Schematic diagram for laser manufacturing of superwetting oil–water separation materials.

3. Superwetting Porous Materials Fabricated by Ultrafast Laser for Oil–Water Separation

3.1. Superoleophilic and Superhydrophobic Porous Materials

Superoleophilic and superhydrophobic materials fabricated by ultrafast lasers play a crucial role in oil–water separation. The unique structures and chemical characteristics of these surfaces enable oil substances to pass through or be adsorbed onto the surfaces while water is completely rejected, thus effectively separating oil from the oil–water mixtures. In general, superoleophilic and superhydrophobic surfaces can be fabricated in two basic ways. The first method involves directly etching or oxidizing the surfaces of the materials through laser beams with high energy density to form micro–nano convex structures or holes, thereby increasing the surface roughness and enhancing the oleophilicity and hydrophobicity of the surfaces. The second method entails fabricating micro–nano structures on the surfaces by laser processing, followed by additional low-surface-energy modification. These strategies, with the different preparation methods, materials, and separation properties mentioned in this chapter, are summarized in Table 1 [106–112].

Recently, numerous laser-processed metal and polymer materials for oil–water separation have been reported. For example, Khan et al. [106] fabricated periodic microstructures on the surfaces of stainless steel and copper mesh by ultrafast laser processing. The superhydrophobic and superoleophilic properties of the processed sample surface were obtained after aging in a vacuum or the air (Figure 6a,b). In oil–water separation tests (Figure 6c), the as-prepared copper mesh exhibited a high permeability for n-hexane, with a separation efficiency of 98%. This environmentally friendly, convenient, chemical-free technique provides guidance for separating oil–water mixtures by laser-structured superoleophilic and superhydrophobic mesh. Additionally, Dong et al. [107] used laser ablation to efficiently, rapidly, and massively induce nanoripple structures on the copper mesh fixed to a PTFE film. The as-prepared copper mesh exhibited superoleophilicity and superhydrophobicity as a result of the formation of the nanoripples through a combined effect of laser ablation of the copper surface as well as resolidification of the ejected PTFE particles (Figure 6d). Furthermore, the copper mesh demonstrated excellent oil–water separation performance in high-temperature, low-temperature, and corrosive environments. Due to the low adhesion, the as-prepared mesh surface also possessed perfect self-cleaning properties (Figure 6e). Yong et al. [108] used laser processing combined with mechanical drilling to create a porous PTFE sheet with durable superoleophilicity and superhydrophobicity. A large number of pores and protrusions were manufactured by laser ablation (Figure 7a). These inherently hydrophobic and rough microstructures endowed PTFE surfaces with excellent superhydrophobic properties. The microhole arrays created by mechanical drilling allowed oil to quickly permeate through the sample surface (Figure 7b). The as-prepared sample exhibited ultralow adsorption to water droplets and a strong attraction to oil (Figure 7c,d). In the oil–water separation tests, the device could efficiently separate oil–water mixtures multiple times (Figure 7e). In addition, the as-prepared sample could also efficiently separate the mixture of oil and strong acid/alkali solutions (Figure 7f). The porous films produced by this method could also work in various harsh environments.

Table 1. Processing parameters and separation properties of superoleophilic/superhydrophobic porous materials.

| Fabrication Methods	Manufacturing Materials	Laser Pulse Duration	Frequency	Energy per Pulse/Laser Power	Scanning Speed (mm/s)	Chemical Modification	Types of Oil	Separation Efficiency (%)	Oil Flux (OF, $Lm^{-2}h^{-1}$)	Characteristics	Refs.
UL processing	Stainless-steel mesh, copper mesh	36 fs	50 kHz	0.1 mJ 5.0 W	100~1200 100, 300	-	n-Hexane	>98	50	Environmentally friendly, chemical free, highly efficient	[106]
UL processing	Copper mesh, PTFE	120 fs	1 kHz	-	0.05	-	Edible oil Glycerol Diesel	~98.3 ~97.9 ~95.8	~46 ~25 ~20	Fast, efficient, self-cleaning ability	[107]
UL processing, mechanical drilling	PTFE	50 fs	1 kHz	20 mW	5	-	Petroleum ether	-	132,840	Simple, durable, stable	[108]
UL processing	Brass sheet	100 ns	20 kHz	0.9 mJ 18 W	500	-	Gasoline Diesel fuel n-Heptane n-Hexane n-Decane Kerosene	~85 ~75 ~90 ~85 ~82 ~90	2880 2160 3240 2880 2520 3240	Facile, economical, environmentally friendly	[109]
UL processing	PTFE	-	200 kHz	4.0 W 20.0 W	1500 150	-	Chloroform Hexadecane Silicon oil Petroleum ether Gasoline Soybean oil	~99.5 ~99.4 ~99.2 ~99.3 ~99.5 ~99.3	~129,960	Facile, rapid, excellent stability and applicability	[110]
Sucrose solution assisted UL	Al film	100 fs	1 kHz	280 μJ 4~16 μJ	0.2 1	PDMS	Dichloroethane	>99.61	19,008	Highly efficient, recyclable, strongly environmental stability	[111]
Needleless electrospinning, reactive laser ablation in liquids	PVDF, PET, Ti foil, $AgNO_3$	400 fs	1 MHz	1.5 μJ 150 mW	2000	KOH	Kitchen oil n-Hexane	97.9 92.3	-	Emulsion separation, eco-friendly	[112]
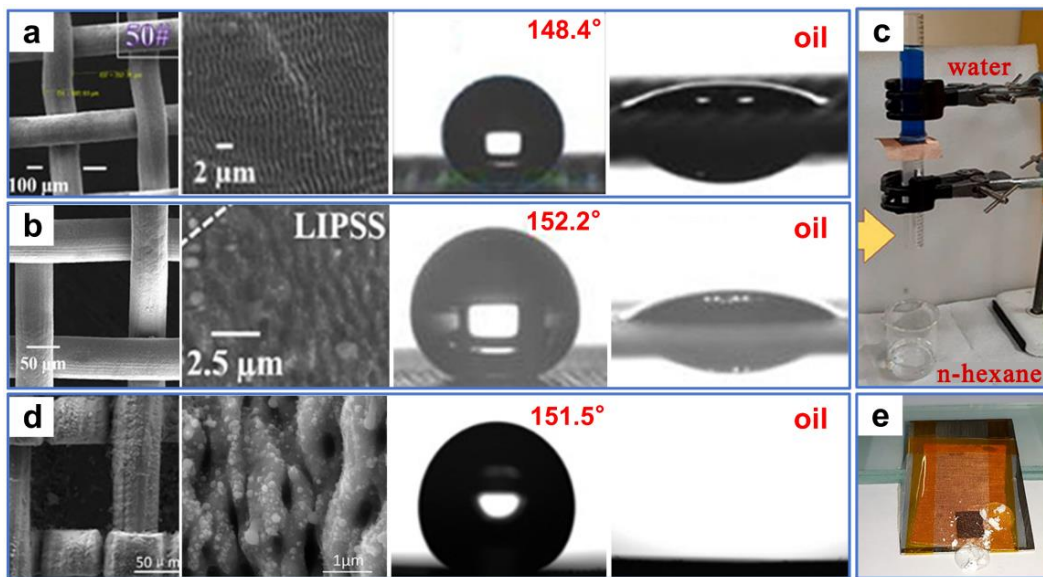
Figure 6. (**a**) SEM images of the stainless-steel meshes before and after processing, water contact-angle, and oil contact-angle measurements of the processed stainless-steel meshes. (**b**) SEM images of the copper meshes before and after processing, water contact-angle, and oil contact-angle measurements of the processed copper meshes. (**c**) Oil–water separation testing of a copper mesh. Reproduced from ref. [106] with permission from Frontiers(copyright 2020). (**d**) SEM images of the as-prepared copper-mesh surface, water contact-angle, and oil contact-angle measurements of the processed copper meshes. (**e**) Self-cleaning tests of the as-prepared mesh. Reproduced from ref. [107] with permission from Elsevier (copyright 2020).
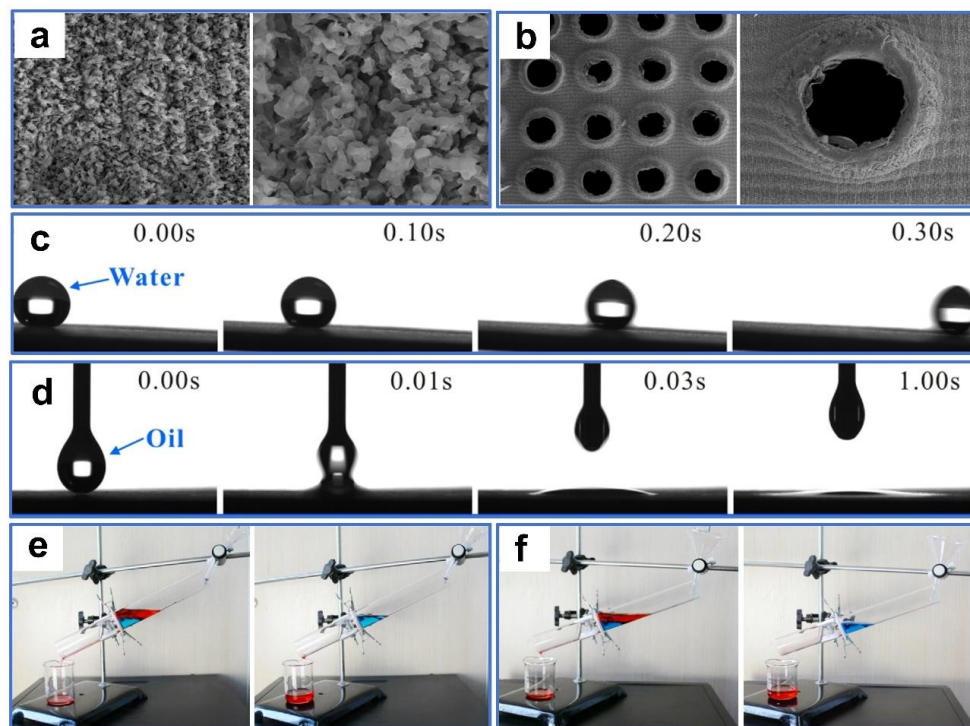

Figure 7. (**a**) SEM images of the PTFE surface after femtosecond laser ablation. (**b**) SEM images of the microholes array structured PTFE sheet. (**c**) A water droplet rolling on the femtosecond laser-ablated surface. (**d**) Dripping an oil droplet on the rough PTFE surface. (**e**) Oil–water separation test of the prepared sample. (**f**) Corrosion resistance test of the prepared sample. Reproduced from ref. [108] with permission from Elsevier (copyright 2016).

Furthermore, ultrafast laser processing can be combined with other surface-modification methods to prepare superhydrophobic and superoleophilic materials. In this case, laser ablation provides a certain surface roughness, while modification imparts opposite wettability to the surface. For instance, Ma et al. [111] fabricated a superhydrophobic and superoleophilic aluminum membrane by combining laser processing and PDMS modification (Figure 8a). First, the parallel narrow slit arrays were neatly fabricated on one side of the Al film along the *x*-axis direction through ultrafast laser processing, with a laser energy density higher than the threshold (Figure 8b). Subsequently, the Al film was immersed in a sucrose solution at a depth of 10 mm, while the other side of the Al film was processed along the *y*-axis direction (Figure 8c). After laser processing, numerous nanospikes were created on the front face of the Al film. Finally, using a muffle furnace, the thin PDMS liquid layer that was spin-coated on the glass substrate was evaporated onto the front side of the Al film. The as-prepared Al film exhibited superhydrophobic/superoleophilic properties and excellent separation efficiency (Figure 8d). In addition, the Al film with excellent stability maintained good superhydrophobicity after 7 months of exposure to air (Figure 8e).
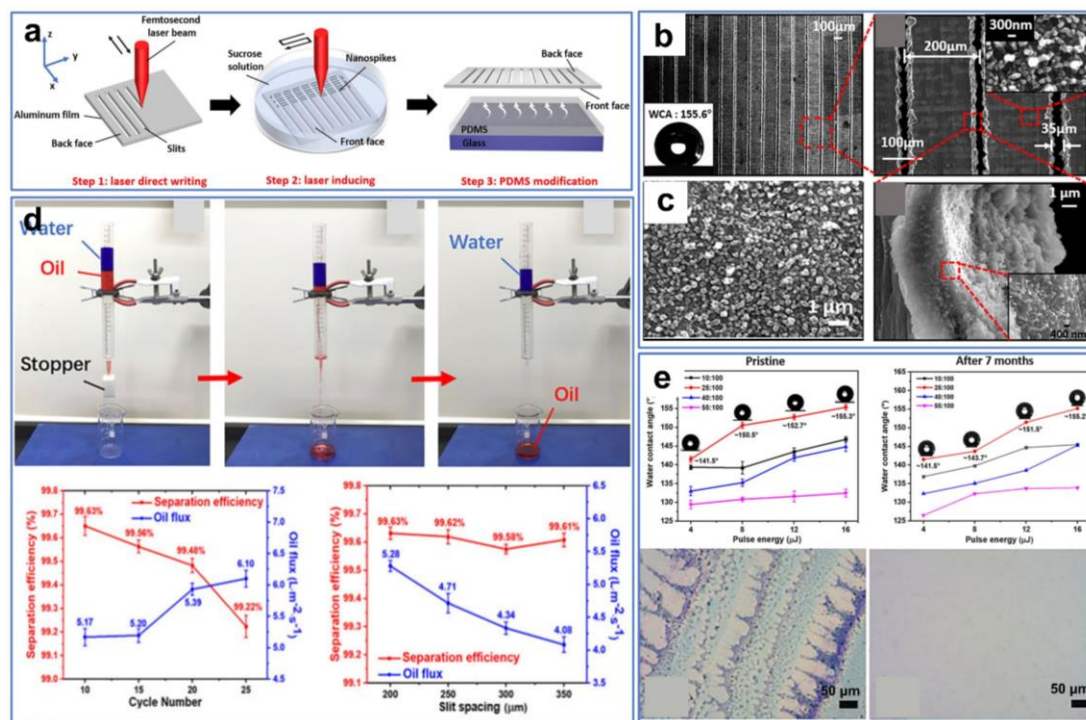

Figure 8. (**a**) Preparation procedure for the Al filter. (**b**) SEM images of the front face of the Al filter with the slit spacing of 200 μm. (**c**) SEM images of nanospikes. (**d**) Oil–water separation testing. (**e**) Durability testing. Reproduced from ref. [111] with permission from Elsevier (copyright 2021).

3.2. Superhydrophilic and Superoleophobic Porous Materials

Superhydrophilic and superoleophobic porous materials, in comparison to superoleophilic and superhydrophobic ones, demonstrate exceptional self-cleaning properties for oil substances by preventing oil contamination and pore plugging. In addition, as a result of the lower density of most oils compared to water, these surfaces exhibit superior gravity-driven separation performance for various oil–water mixtures. In recent years, significant breakthroughs have been achieved in removing oil from oil–water mixtures using ultrafast laser-fabricated superhydrophilic and superoleophobic porous materials. The preparation methods, materials, and separation performances of the strategies mentioned in this chapter are summarized in Table 2 [113–120].

Table 2. Processing parameters and separation properties of superhydrophilic/superoleophobic porous materials.

Fabrication Methods	Manufacturing Materials	Laser Pulse Duration	Frequency	Energy per Pulse/Laser Power	Scanning Speed (mm/s)	Types of Oil	Separation Efficiency (%)	Water Flux (WF, $Lm^{-2}h^{-1}$)	Characteristics	Refs.
UL processing	Stainless-steel mesh	100 ns	50 kHz	12 W	500	Kerosene Peanut oil	~97.7 ~97.3	>63,000	Simple, economical, high efficiency	[113]
UL processing	Stainless-steel mesh, soda lime glass	200 ns	18 kHz	1~2.5 W	5	Mustard oil Kerosene Petrol	~97.5 ~97 ~97.1	~145,000	Simple, high efficiency, stable	[114]
UL processing	Stainless-steel mesh, Cu foil	100 ns	20 kHz	10 W	500	Kerosene Soybean oil Hexadecane Dodecane Silicone oil	~98.5 ~96.8 ~97.5 ~97.3 ~96.6	~118,800	Fast, efficient, self-cleaning	[115]
UL processing	Al foil	104 fs	1 kHz	50 μJ	-	1,2-Dichloroethane Normal octane	99	77,000	High speed, efficient	[116]
UL processing, mechanical drilling	Iron sheet	50 fs	1 kHz	30 mW	6	1,2-Dichloroethane	>97.8	-	Widely applicable	[117]
UL processing	Al alloy, Ti alloy, stainless steel	100 ns	20 kHz	14 W	500	Kerosene Soybean oil Sesame oil	~97.8 ~97.5	-	Large area, durable	[118]
UL processing	Cu foil	5 ns	90 kHz	-	5	Hexane Toluene	~98	~16,000	Simple, efficient, scalable	[119]
UL processing	Eggshell membrane	-	25 kHz	0.193 W 1.32 W	800	Peanut oil Toluene Petroleum ether Paraffin oil	~98.7 ~99.2 ~98.7 ~98.6	~12,500 ~16,500 ~22,500 ~11,000	Green, anti-corrosion, robust, self-cleaning	[120]

For example, Yu et al. [113] fabricated a superhydrophilic/superoleophobic stainless-steel mesh by ultrafast laser treatment. Abundant micron-sized grit structures were created on the smooth stainless-steel surface (Figure 9a,b), and these rough structures were mainly oxides with hydrophilicity. The superwettability of the laser-treated stainless-steel mesh was predominantly attributed to these micro–nano structures and oxides. After laser processing, the surface wettability changed from hydrophobic and underwater oleophobic to superhydrophilic and underwater superoleophobic (Figure 9c,d). This alteration in wettability endowed the surface with excellent oil-blocking oil–water separation properties. Similarly, Ahlawat et al. [114] used a nanosecond laser to induce the deposition of glass particles on the stainless-steel mesh, creating long-term superhydrophilic micro–nano structures and enabling gravity-driven oil–water separation (Figure 9e,f). This chemical-free and one-step processing method holds significance for environmental conservation.
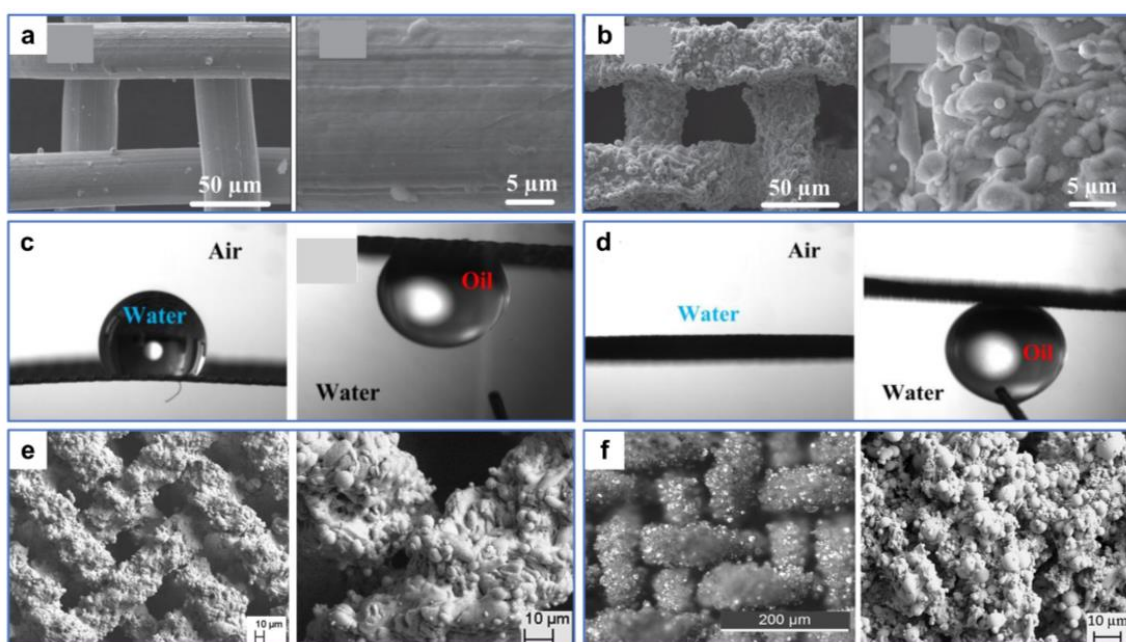

Figure 9. (**a**) SEM images of the untreated stainless-steel mesh surface. (**b**) SEM images of the treated stainless-steel mesh surface. (**c**) Wettability test of the untreated stainless-steel mesh. (**d**) Wettability test of the treated stainless-steel mesh. Reproduced from ref. [113] with permission from IOP Publishing (copyright 2018). (**e**) SEM images of the laser texturing without any glass plate. (**f**) SEM images of the laser-textured mesh covered with soda lime glass plate during laser processing. Reproduced from ref. [114] with permission from Elsevier (copyright 2021).

Additionally, the pores of materials designed for oil–water separation can be directly manufactured by ultrafast laser. For instance, Li et al. [116] fabricated ultrathin Al foil with large-area regular micropore arrays by one-step laser processing. Leveraging high precision and controllability, the uniform arrays of micropores with rough nanostructures were neatly arranged on the surface of the aluminum foil by a femtosecond laser (Figure 10a). The multi-stage composite structures provided by micro-sized pores and nanoscale roughness greatly changed the wettability of the aluminum foil from hydrophilic to superhydrophilic and underwater superoleophobic (Figure 10b). By employing a small oil–water separator, substantial quantities of light and heavy oil–water mixtures could be easily and quickly separated and purified, offering the potential for recovering oil and water (Figure 10c). In addition, the micropore-arrayed aluminum foil can efficiently filter particles of different sizes (Figure 10d), demonstrating versatile application properties. The as-prepared controllable aluminum foils with high precision and efficiency provide an alternative for building a lab-on-a-chip and even separating blood and cells.
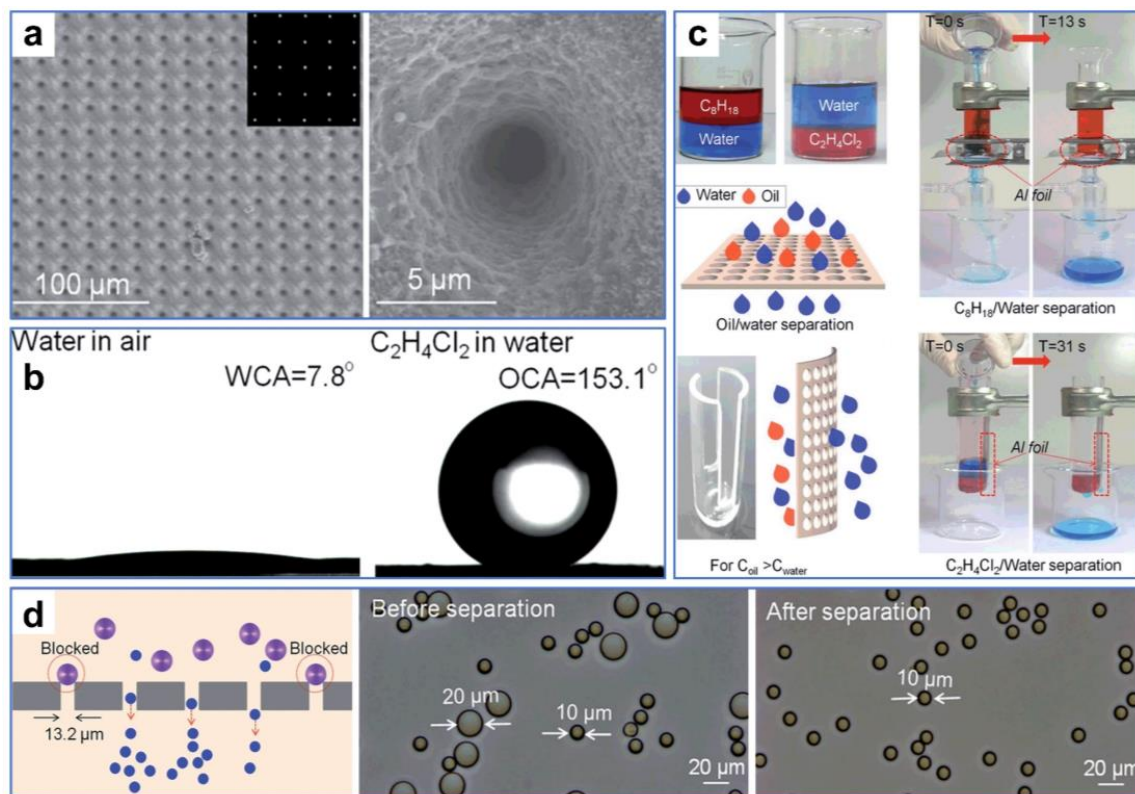
Figure 10. (**a**) SEM images of the as-prepared ultrathin Al foil. (**b**) Wettability test of the treated Al foil. (**c**) Oil–water separation treatment of the treated Al foil. (**d**) Filtration performance test of the treated Al foil. Reproduced from ref. [116] with permission from The Royal Society of Chemistry; Royal Society of Chemistry (copyright 2016).

In addition to laser-fabricated metal membranes, nonmetal porous materials with superwettability can also be produced by ultrafast lasers for oil–water separation. For example, Xia et al. [120] used a simple and environmentally friendly laser-processing strategy to prepare superhydrophilic and superoleophobic membranes for oil–water separation from discarded eggshells and eggshell membranes (Figure 11a). Due to the abundant hydrophilic groups of this organic biomaterial, such as hydroxyl, amino, and carboxyl groups, coupled with the multilevel micro–nano structures created by laser processing, the as-prepared membranes exhibit strong superhydrophilicity and underwater superoleophobicity (Figure 11b). In dynamic wettability tests of the membranes, both light and heavy oils were able to slide on the very lowly inclined surfaces, indicating the strong oil-rejection properties of the as-prepared membranes (Figure 11c). In addition, the as-prepared membranes demonstrated excellent self-cleaning and anti-contamination capabilities. Despite being prewetted by oil, the $\Delta P < 0$ is for both water and oil under this condition. Consequently, the water was able to clean the oil and permeate the membrane, leading to the failure of oil–water separation (Figure 11d). However, for the water-prewetted membrane, the $\Delta P < 0$ is for water, while the $\Delta P > 0$ is for oil. In this case, water could pass through the membrane while oil could not, thus successfully realizing oil-blocking oil–water separation (Figure 11e). These laser-engineered eggshell membranes with green, durable, and self-cleaning properties serve as a commendable example of utilizing bio-wastes in oil–water separation.
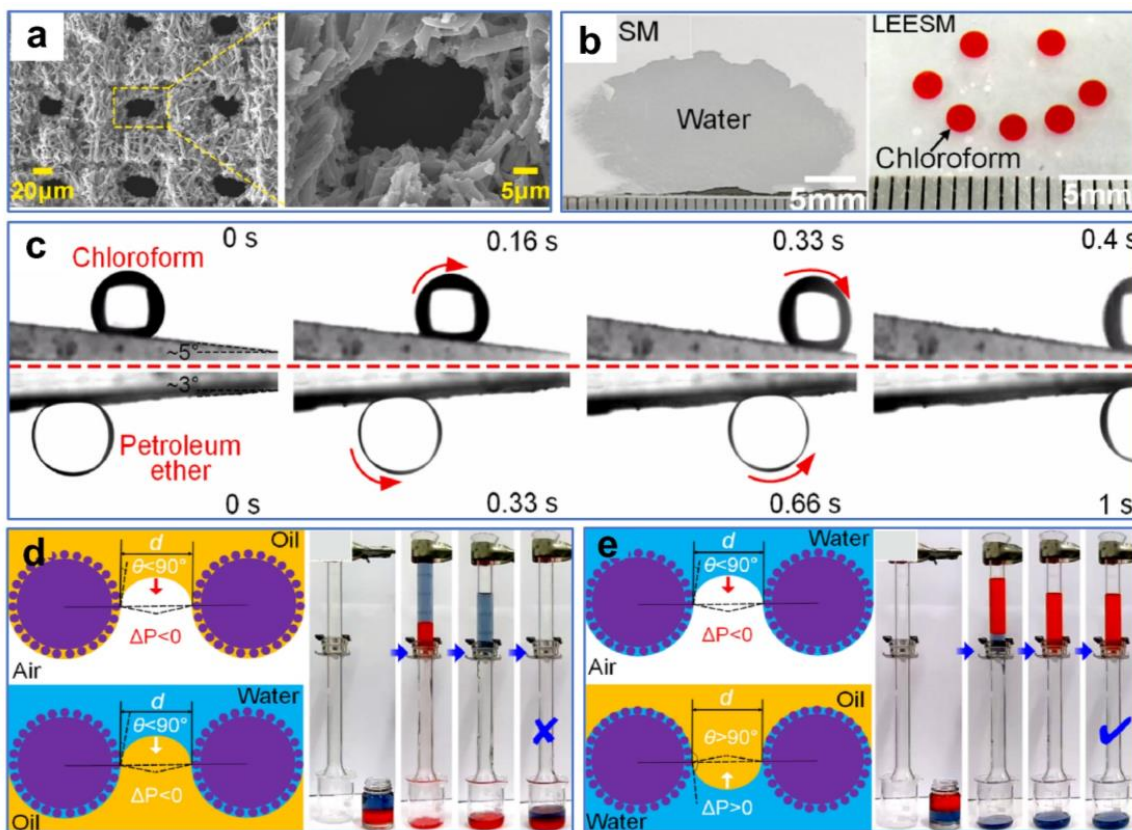
Figure 11. (**a**) SEM images of the as-prepared membranes. (**b**) Wettability of the as-prepared membranes. (**c**) Time-lapsed snapshots of chloroform and petroleum ether droplets rolling off the tilted samples in water. (**d**) Oil–water separation test with oil pre-wetting. (**e**) Oil–water separation test with water pre-wetting. Reproduced from ref. [120] with permission from Elsevier (copyright 2022).

3.3. Superwetting Porous Materials with Reversible or Superamphiphilic Wettability

In the above discussion, it can be seen that the superoleophilic/superhydrophobic porous materials and superhydrophilic/superoleophobic porous materials are limited to separating oil or water from oil–water mixtures. These two strategies lack flexibility, as they cannot selectively separate oil and water from the mixtures in different applications and conditions. Specifically, superhydrophobic/superoleophilic materials may separate heavy oils (density larger than that of water) from the mixtures while not effectively separating light oils (density larger than that of water). Hence, developing materials with switchable wettability is of great significance, and an ultrafast laser provides a powerful tool for addressing these issues by effectively altering the surface wettability. The preparation methods, materials, and separation properties of the reported strategies for multiuse separation mentioned in this chapter are summarized in Table 3 [121–126].

Table 3. Processing parameters and separation properties of reversible superwetting porous materials.

Fabrication Methods	Manufacturing Materials	Laser Pulse Duration	Frequency	Energy per Pulse/Laser Power	Scanning Speed (mm/s)	Wettability Transformation Methods	Types of Oil	Separation Efficiency (%)	Oil–Water Flux (Lm^{-2}h^{-1})	Characteristics	Refs.
UL processing	Stainless-steel mesh	100 ns	-	12 W	500	Ethanol soaking, natural drying	Kerosene Lubricating oil Dichloromethane Dichloroethane	~96 ~96.7 ~97 ~96.3	WF ≈ 102,600	Facile, economical, environmentally friendly	[121]
UL processing	PDMS, curing agent, Al sheets	-	-	6 W	800	APPJ treatment, heating treatment	Dichloromethane Peanut oil Diesel Hexadecane Lubricating oil	~96 ~97.5 ~99 ~97.3 ~98	OF ≈ 15,000 WF ≈ 18,000	Environmentally friendly, low cost, high efficiency	[122]
Waterjet-assisted laser ablation, UL processing	Stainless-steel mesh	100 ns	-	18 W	200	-	Kerosene Soybean oil n-Heptane Dichloromethane 1,2-Dichloroethane	~97.6 ~96.9 ~98.3 ~97.5 ~97.5	-	Simple, environmentally friendly, excellent mechanical property	[123]
UL processing	Brass mesh	100 ns	20 kHz	10 W	500	-	Kerosene Soybean oil Dodecane 1,2-Dichloroethane Chloroform	~98.5 ~96.4 ~97 ~96.3 ~98	WF > 134,280 OF > 76,680	Simple, high efficiency, stable	[124]
UL processing	Copper sheet	100 ns	-	24 W	1000	-	Kerosene Isooctane Heptane 1,2-Dichloroethane Dichloromethane	>98	WF > 32,000 OF > 37,500	Superior environmental stability	[125]
UL processing, chemical modification	Cu wire mesh, fluorosilane, GO	-	-	100 mW	2	-	Bean oil n-Heptane Methylbenzene Perchlormethane Trichloromethane	-	-	Asymmetric wettability	[126]

Wang et al. [121] processed stainless-steel mesh with a nanosecond laser and obtained reversible surface wettability induced by ethanol. The smart surface with good mechanical durability and environmental stability could efficiently separate both light and heavy oil–water mixtures. The nearly smooth original substrate was processed by laser to obtain many micron-sized sand structures and nanoscale fluffy structures (Figure 12a,b). The wettability of the stainless-steel mesh changed from hydrophobicity/superoleophilicity to superhydrophilicity/superoleophilicity after processing. As the time the sample was exposed to air increased, the wettability of the meshes changed from superhydrophilic to superhydrophobic due to the accumulation of nonpolar carbon on the rough surfaces. The surface wettability of the meshes could be reversed by ethanol soaking and natural drying treatments, and this conversion allows efficient separation for both light and heavy oil–water mixtures (Figure 12c). The theoretical explanation for this phenomenon was that the pristine surfaces without ethanol modification were superhydrophobic/superoleophilic, so heavy oil could pass through the surfaces while water could not (Figure 12d). In contrast, surfaces treated with ethanol were superhydrophilic/underwater superoleophobic. Thus, water could pass through the surfaces while light oil was blocked (Figure 12e).
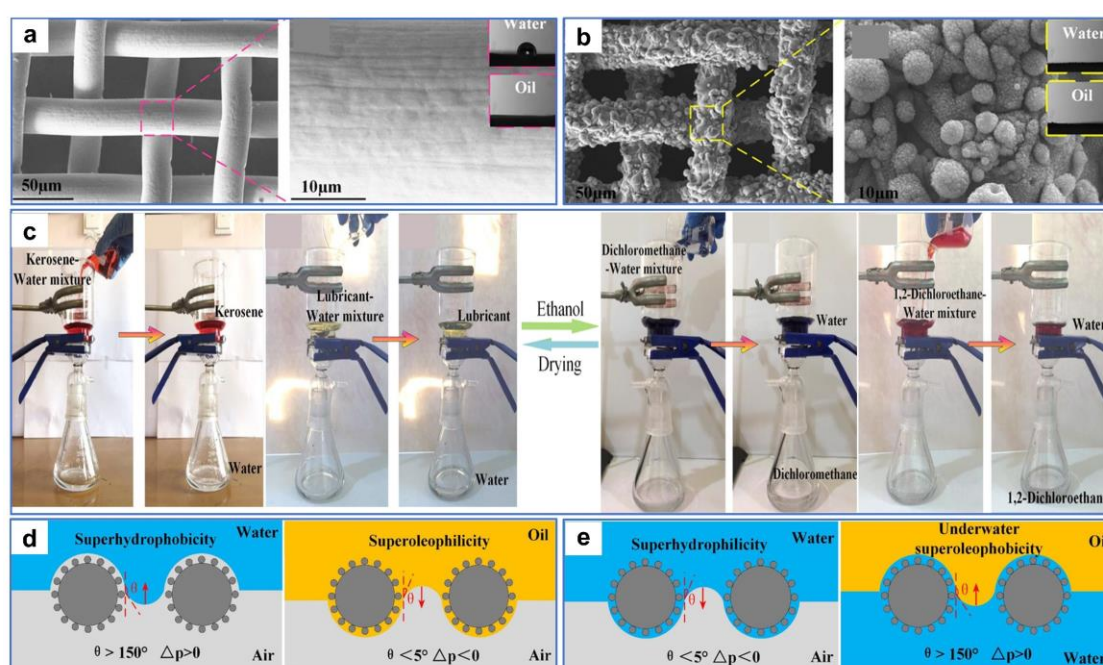

Figure 12. (**a**) SEM images of the original stainless-steel mesh. (**b**) SEM images of the processed stainless-steel mesh. (**c**) Digital images of the separation process of light oil–water mixtures (**left**) and heavy oil–water mixtures (**right**). (**d**,**e**) Schematic of the oil–water mixtures' separation mechanism. Reproduced from ref. [121] with permission from American Chemical Society (copyright 2020).

While the oil–water separation materials with reversible superwettability can be obtained via treatments, such as ethanol immersion, atmospheric pressure plasma jet [122], etc., these methods may entail additional expense or complex conversion operations in practical applications. Therefore, superamphiphilic membranes with superhydrophilic and superoleophilic properties may have a wider range of practical applications. For example, Wang et al. [123] fabricated a robust microstructure on 304 stainless-steel mesh using waterjet-assisted laser ablation. The as-prepared mesh showed excellent separation performances for light and heavy oil–water mixtures and corrosion solutions–oil mixtures. As shown in Figure 13a, the surface of the original stainless-steel mesh without microstructures and micropores is relatively smooth. After treatment, abundant micron-sized sandy textures and micropores were created on the mesh surface, and the pore size was reduced (Figure 13b). These micro–nano structures played a crucial part in the superwettability

of the mesh surface. Water and oil droplets diffused rapidly upon contacting the sample surface, indicating the superhydrophilic and superoleophilic properties of the processed surface (Figure 13c). In liquid environments, the wettability of the mesh changed from underwater oleophobic and underoil superhydrophobic to underwater superoleophobic and underoil superhydrophobic after processing (Figure 13d,e). The as-prepared stainless-steel mesh could achieve the separation for light and heavy oil–water mixtures only by water prewetting and oil prewetting. When the as-prepared mesh was prewetted by water, the water could pass quickly through the mesh, while the light oil could not. In contrast, when the mesh was prewetted by oil, the heavy oil could pass quickly through the mesh, while the water could not.
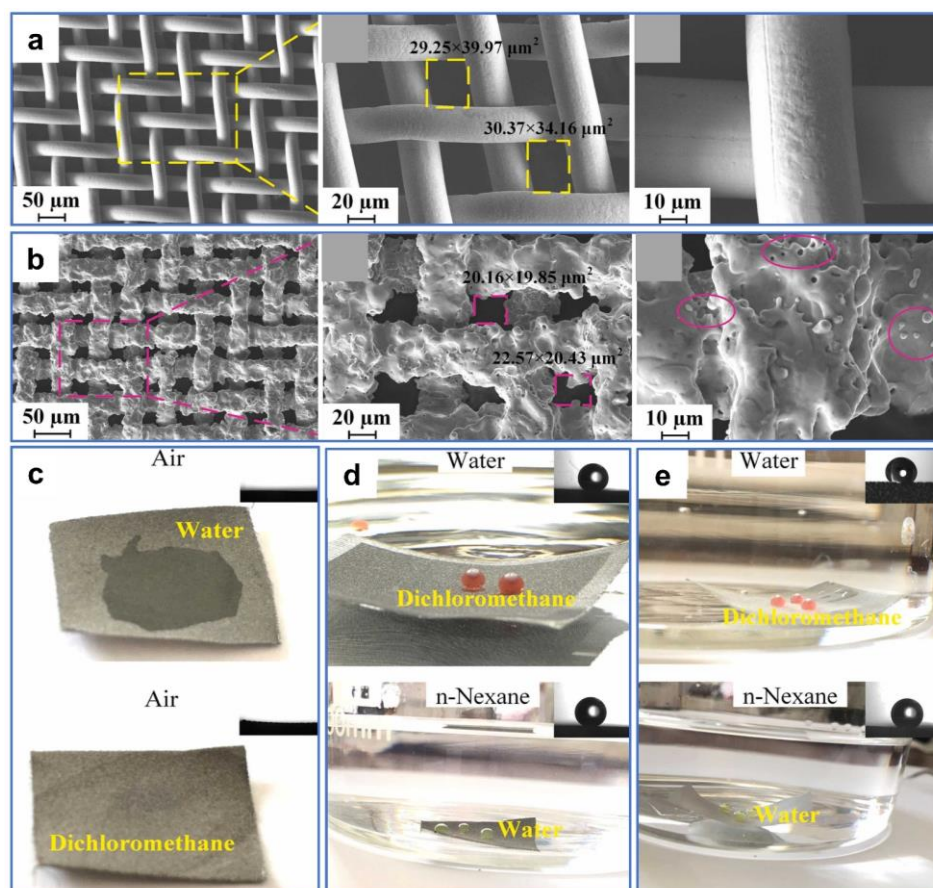

Figure 13. (**a**) SEM images of the original stainless-steel mesh. (**b**) SEM images of the processed stainless-steel mesh. (**c**) Digital images and contact angles of water and oil droplets on the as-prepared stainless-steel mesh in the air. (**d**) Digital images and contact angles of underwater oil droplets and underoil water droplets on the as-prepared stainless-steel mesh. (**e**) Digital images and contact angles of underwater oil droplets and underoil water droplets on the original stainless-steel mesh. Reproduced from ref. [123] with permission from Elsevier (copyright 2022).

4. Summary and Outlooks

The substantial discharge of oily wastewater and frequent oil spills pose significant threats to the ecosystem and the economy. Therefore, the development of materials for efficient oil–water separation holds great potential for practical applications. Ultrafast lasers have attracted widespread attention from researchers due to their high processing precision, facile operating procedures, and broad processability of various existing materials. The surface morphology and chemical composition of materials can be effectively controlled by laser-manufactured micro–nano structures, which dramatically change the properties of the material. Inspired by numerous natural superwetting surfaces, the bionic laser-processed porous materials with superwetting properties, includ-

ing superoleophilic/superhydrophobic materials for water-blocking separation, superhydrophilic/superoleophobic materials for oil-blocking separation, superamphiphilic materials for on-demand oil–water separation, etc., have been further developed. This demonstrates the tremendous application potential of these laser-manufacturing strategies in practical multi-purpose oil–water separation.

However, there are still several issues associated with ultrafast laser-fabricated superwetting porous materials for oil–water separation. First, the current separation materials may face challenges in terms of mechanical and chemical stability. Therefore, developing separation materials with high durability and recyclability is essential to facilitate their large-scale applications. Second, research on the interaction mechanism between ultrafast lasers and various metallic and non-metallic materials is not comprehensive enough, which significantly limits the application of femtosecond laser processing in new materials for multiple uses. In addition, the relationship between different laser-induced surface micro/nanostructures, such as nanospike arrays and microgrooves, and the corresponding wetting properties have not been fully revealed, which could be focused on in the future. In addition, there is a lack of uniform characterization methods for the oil–water separation performances of the fabricated materials, such as the testing equipment and calculation methods for separation efficiency tests, filtrate volume and operation methods for flux tests, types of used oil models for separation, etc., which is not conducive to evaluate different preparation strategies. In summary, while ultrafast laser processing still faces challenges, it offers a promising alternative in biomimetic micro/nanosurface fabrication. With the refinement of the theoretical system of ultrafast laser processing, it is anticipated that the purification technology for separating complex oil–water mixtures containing multiple components will witness significant advancements.

Author Contributions: W.X. and L.Z. contributed equally to this work. W.X. and L.Z.: Methodology, Analysis, Writing-Original Draft. R.J.: Resources, Supervision. C.C.: Conceptualization, Funding Acquisition, Supervision, Writing—Review & Editing. All authors have read and agreed to the published version of the manuscript.

Data Availability Statement: Data availability is not applicable to this article as no new data were created or analyzed in this study.

Conflicts of Interest: The authors declare no conflicts of interest.

References

1. Govindarajan, S.K.; Mishra, A.; Kumar, A. Oil spill in a marine environment: Requirements following an offshore oil spill. *Rud. Geološko Naft. Zb.* **2021**, *36*, 1–9. [CrossRef]
2. Ismail, N.H.; Salleh, W.N.W.; Ismail, A.F.; Hasbullah, H.; Yusof, N.; Aziz, F.; Jaafar, J. Hydrophilic Polymer-Based Membrane for Oily Wastewater Treatment: A Review. *Sep. Purif. Technol.* **2020**, *233*, 116007. [CrossRef]
3. Sutrisna, P.D.; Kurnia, K.A.; Siagian, U.W.R.; Ismadji, S.; Wenten, I.G. Membrane Fouling and Fouling Mitigation in Oil–Water Separation: A Review. *J. Environ. Chem. Eng.* **2022**, *10*, 107532. [CrossRef]
4. Chu, Z.; Feng, Y.; Seeger, S. Oil/Water Separation with Selective Superantiwetting/Superwetting Surface Materials. *Angew. Chem. Int. Ed.* **2015**, *54*, 2328–2338. [CrossRef] [PubMed]
5. Cao, X.; Chang, Y.-C. A Two-Dimensional Assessment of China's Approach Concerning the Compensation Fund for Ship-Induced Oil Pollution Damage: Pollution Governance and Victim Compensation. *Front. Mar. Sci.* **2022**, *9*, 817049. [CrossRef]
6. Aseev, N.A.; Agoshkov, V.I.; Zalesny, V.B.; Aps, R.; Kujala, P.; Rytkönen, J. The Problem of Control of Oil Pollution Risk in the Baltic Sea. *Russ. J. Numer. Anal. Math. Model.* **2014**, *29*, 93–105. [CrossRef]
7. Sauer, T.C.; Brown, J.S.; Boehm, P.D.; Aurand, D.V.; Michel, J.; Hayes, M.O. Hydrocarbon Source Identification and Weathering Characterization of Intertidal and Subtidal Sediments along the Saudi Arabian Coast after the Gulf War Oil Spill. *Mar. Pollut. Bull.* **1993**, *27*, 117–134. [CrossRef]

8. Bruckberger, M.C.; Morgan, M.J.; Bastow, T.P.; Walsh, T.; Prommer, H.; Mukhopadhyay, A.; Kaksonen, A.H.; Davis, G.B.; Puzon, G.J. Investigation into the Microbial Communities and Associated Crude Oil-Contamination along a Gulf War Impacted Groundwater System in Kuwait. *Water Res.* **2020**, *170*, 115314. [CrossRef] [PubMed]

9. Bejarano, A.C.; Michel, J. Large-Scale Risk Assessment of Polycyclic Aromatic Hydrocarbons in Shoreline Sediments from Saudi Arabia: Environmental Legacy after Twelve Years of the Gulf War Oil Spill. *Environ. Pollut.* **2010**, *158*, 1561–1569. [CrossRef]

10. Readman, J.W.; Fowler, S.W.; Villeneuve, J.-P.; Cattini, C.; Oregioni, B.; Mee, L.D. Oil and Combustion-Product Contamination of the Gulf Marine Environment Following the War. *Nature* **1992**, *358*, 662–665. [CrossRef]

11. Michel, J.; Owens, E.H.; Zengel, S.; Graham, A.; Nixon, Z.; Allard, T.; Holton, W.; Reimer, P.D.; Lamarche, A.; White, M.; et al. Extent and Degree of Shoreline Oiling: Deepwater Horizon Oil Spill, Gulf of Mexico, USA. *PLoS ONE* **2013**, *8*, e65087. [CrossRef]

12. Valentine, D.L.; Fisher, G.B.; Bagby, S.C.; Nelson, R.K.; Reddy, C.M.; Sylva, S.P.; Woo, M.A. Fallout Plume of Submerged Oil from *Deepwater Horizon*. *Proc. Natl. Acad. Sci. USA* **2014**, *111*, 15906–15911. [CrossRef]

13. Kujawinski, E.B.; Kido Soule, M.C.; Valentine, D.L.; Boysen, A.K.; Longnecker, K.; Redmond, M.C. Fate of Dispersants Associated with the Deepwater Horizon Oil Spill. *Environ. Sci. Technol.* **2011**, *45*, 1298–1306. [CrossRef]

14. Reddy, C.M.; Arey, J.S.; Seewald, J.S.; Sylva, S.P.; Lemkau, K.L.; Nelson, R.K.; Carmichael, C.A.; McIntyre, C.P.; Fenwick, J.; Ventura, G.T.; et al. Composition and Fate of Gas and Oil Released to the Water Column during the *Deepwater Horizon* Oil Spill. *Proc. Natl. Acad. Sci. USA* **2012**, *109*, 20229–20234. [CrossRef] [PubMed]

15. Korshunova, T.Y.; Chetverikov, S.P.; Bakaeva, M.D.; Kuzina, E.V.; Rafikova, G.F.; Chetverikova, D.V.; Loginov, O.N. Microorganisms in the Elimination of Oil Pollution Consequences (Review). *Appl. Biochem. Microbiol.* **2019**, *55*, 344–354. [CrossRef]

16. Dijkstra, A. Integrated Pollution Control in Seed Oil Refining. *Fett/Lipid* **1999**, *101*, 132–137. [CrossRef]

17. Dai, X.; Lv, J.; Fu, P.; Guo, S. Microbial Remediation of Oil-Contaminated Shorelines: A Review. *Environ. Sci. Pollut. Res.* **2023**, *30*, 93491–93518. [CrossRef] [PubMed]

18. Renegar, D.A.; Schuler, P.A.; Knap, A.H.; Dodge, R.E. TRopical Oil Pollution Investigations in Coastal Systems [TROPICS]: A Synopsis of Impacts and Recovery. *Mar. Pollut. Bull.* **2022**, *181*, 113880. [CrossRef] [PubMed]

19. Wolok, E.; Barafi, J.; Joshi, N.; Girimonte, R.; Chakraborty, S. Study of Bio-Materials for Removal of the Oil Spill. *Arab. J. Geosci.* **2020**, *13*, 1244. [CrossRef]

20. Chen, J.; Zhang, W.; Wan, Z.; Li, S.; Huang, T.; Fei, Y. Oil Spills from Global Tankers: Status Review and Future Governance. *J. Clean. Prod.* **2019**, *227*, 20–32. [CrossRef]

21. Frising, T.; Noïk, C.; Dalmazzone, C. The Liquid/Liquid Sedimentation Process: From Droplet Coalescence to Technologically Enhanced Water/Oil Emulsion Gravity Separators: A Review. *J. Dispers. Sci. Technol.* **2006**, *27*, 1035–1057. [CrossRef]

22. Li, B.; Qi, B.; Guo, Z.; Wang, D.; Jiao, T. Recent Developments in the Application of Membrane Separation Technology and Its Challenges in Oil-Water Separation: A Review. *Chemosphere* **2023**, *327*, 138528. [CrossRef] [PubMed]

23. Wang, D.; Zhao, Z.; Qiao, C.; Yang, W.; Huang, Y.; McKay, P.; Yang, D.; Liu, Q.; Zeng, H. Techniques for Treating Slop Oil in Oil and Gas Industry: A Short Review. *Fuel* **2020**, *279*, 118482. [CrossRef]

24. Borja, R.; Raposo, F.; Rincón, B. Treatment Technologies of Liquid and Solid Wastes from Two-Phase Olive Oil Mills. *Grasas y Aceites* **2006**, *57*, 32–46. [CrossRef]

25. Ge, J.; Zong, D.; Jin, Q.; Yu, J.; Ding, B. Biomimetic and Superwettable Nanofibrous Skins for Highly Efficient Separation of Oil-in-Water Emulsions. *Adv. Funct. Mater.* **2018**, *28*, 1705051. [CrossRef]

26. Chen, C.; Weng, D.; Mahmood, A.; Chen, S.; Wang, J. Separation Mechanism and Construction of Surfaces with Special Wettability for Oil/Water Separation. *ACS Appl. Mater. Interfaces* **2019**, *11*, 11006–11027. [CrossRef] [PubMed]

27. Kang, S.M.; Choi, J.S.; An, J.H. Reliable and Robust Fabrication Rules for Springtail-Inspired Superomniphobic Surfaces. *ACS Appl. Mater. Interfaces* **2020**, *12*, 21120–21126. [CrossRef]

28. Hensel, R.; Finn, A.; Helbig, R.; Braun, H.-G.; Neinhuis, C.; Fischer, W.-J.; Werner, C. Biologically Inspired Omniphobic Surfaces by Reverse Imprint Lithography. *Adv. Mater.* **2014**, *26*, 2029–2033. [CrossRef]

29. Yun, G.-T.; Jung, W.-B.; Oh, M.S.; Jang, G.M.; Baek, J.; Kim, N.I.; Im, S.G.; Jung, H.-T. Springtail-Inspired Superomniphobic Surface with Extreme Pressure Resistance. *Sci. Adv.* **2018**, *4*, eaat4978. [CrossRef]

30. Ensikat, H.J.; Ditsche-Kuru, P.; Neinhuis, C.; Barthlott, W. Superhydrophobicity in Perfection: The Outstanding Properties of the Lotus Leaf. *Beilstein J. Nanotechnol.* **2011**, *2*, 152–161. [CrossRef]

31. Li, X.; Gong, F.; Liu, D.; He, S.; Yuan, H.; Dai, L.; Cai, X.; Liu, J.; Guo, J.; Jin, Y.; et al. A Lotus Leaf Based Random Laser. *Org. Electron.* **2019**, *69*, 216–219. [CrossRef]

32. Barthlott, W.; Schimmel, T.; Wiersch, S.; Koch, K.; Brede, M.; Barczewski, M.; Walheim, S.; Weis, A.; Kaltenmaier, A.; Leder, A.; et al. The Salvinia Paradox: Superhydrophobic Surfaces with Hydrophilic Pins for Air Retention Under Water. *Adv. Mater.* **2010**, *22*, 2325–2328. [CrossRef] [PubMed]

33. Li, X.; Yang, J.; Lv, K.; Papadopoulos, P.; Sun, J.; Wang, D.; Zhao, Y.; Chen, L.; Wang, D.; Wang, Z.; et al. Salvinia-like Slippery Surface with Stable and Mobile Water/Air Contact Line. *Natl. Sci. Rev.* **2021**, *8*, nwaa153. [CrossRef] [PubMed]

34. Zhang, X.; Sun, L.; Wang, Y.; Bian, F.; Wang, Y.; Zhao, Y. Multibioinspired Slippery Surfaces with Wettable Bump Arrays for Droplets Pumping. *Proc. Natl. Acad. Sci. USA* **2019**, *116*, 20863–20868. [CrossRef] [PubMed]

35. Chen, H.; Zhang, P.; Zhang, L.; Liu, H.; Jiang, Y.; Zhang, D.; Han, Z.; Jiang, L. Continuous Directional Water Transport on the Peristome Surface of Nepenthes Alata. *Nature* **2016**, *532*, 85–89. [CrossRef]

36. Zheng, Y.; Bai, H.; Huang, Z.; Tian, X.; Nie, F.-Q.; Zhao, Y.; Zhai, J.; Jiang, L. Directional Water Collection on Wetted Spider Silk. *Nature* **2010**, *463*, 640–643. [CrossRef] [PubMed]

37. Feng, S.; Zhu, P.; Zheng, H.; Zhan, H.; Chen, C.; Li, J.; Wang, L.; Yao, X.; Liu, Y.; Wang, Z. Three-Dimensional Capillary Ratchet-Induced Liquid Directional Steering. *Science* **2021**, *373*, 1344–1348. [CrossRef] [PubMed]

38. Feng, L.; Zhang, Y.; Xi, J.; Zhu, Y.; Wang, N.; Xia, F.; Jiang, L. Petal Effect: A Superhydrophobic State with High Adhesive Force. *Langmuir* **2008**, *24*, 4114–4119. [CrossRef]

39. Liu, M.; Wang, S.; Wei, Z.; Song, Y.; Jiang, L. Bioinspired Design of a Superoleophobic and Low Adhesive Water/Solid Interface. *Adv. Mater.* **2009**, *21*, 665–669. [CrossRef]

40. Nishimoto, S.; Bhushan, B. Bioinspired Self-Cleaning Surfaces with Superhydrophobicity, Superoleophobicity, and Superhydrophilicity. *RSC Adv.* **2012**, *3*, 671–690. [CrossRef]

41. Si, Y.; Dong, Z.; Jiang, L. Bioinspired Designs of Superhydrophobic and Superhydrophilic Materials. *ACS Cent. Sci.* **2018**, *4*, 1102–1112. [CrossRef]

42. Jiang, T.; Guo, Z.; Liu, W. Biomimetic Superoleophobic Surfaces: Focusing on Their Fabrication and Applications. *J. Mater. Chem. A* **2015**, *3*, 1811–1827. [CrossRef]

43. Zhang, S.; Huang, J.; Chen, Z.; Lai, Y. Bioinspired Special Wettability Surfaces: From Fundamental Research to Water Harvesting Applications. *Small* **2017**, *13*, 1602992. [CrossRef]

44. Park, K.-C.; Kim, P.; Grinthal, A.; He, N.; Fox, D.; Weaver, J.C.; Aizenberg, J. Condensation on Slippery Asymmetric Bumps. *Nature* **2016**, *531*, 78–82. [CrossRef]

45. Yong, J.; Yang, Q.; Hou, X.; Chen, F. Emerging Separation Applications of Surface Superwettability. *Nanomaterials* **2022**, *12*, 688. [CrossRef]

46. Bai, X.; Yuan, Z.; Lu, C.; Zhan, H.; Ge, W.; Li, W.; Liu, Y. Recent Advances in Superwetting Materials for Separation of Oil/Water Mixtures. *Nanoscale* **2023**, *15*, 5139–5157. [CrossRef] [PubMed]

47. Wang, L.; Gong, Q.; Zhan, S.; Jiang, L.; Zheng, Y. Robust Anti-Icing Performance of a Flexible Superhydrophobic Surface. *Adv. Mater.* **2016**, *28*, 7729–7735. [CrossRef]

48. Darmanin, T.; Guittard, F. Superhydrophobic and Superoleophobic Properties in Nature. *Mater. Today* **2015**, *18*, 273–285. [CrossRef]

49. Wang, D.-C.; Yang, X.; Yu, H.-Y.; Gu, J.; Qi, D.; Yao, J.; Ni, Q. Smart Nonwoven Fabric with Reversibly Dual-Stimuli Responsive Wettability for Intelligent Oil-Water Separation and Pollutants Removal. *J. Hazard. Mater.* **2020**, *383*, 121123. [CrossRef]

50. Wang, Y.; Gong, X. Special Oleophobic and Hydrophilic Surfaces: Approaches, Mechanisms, and Applications. *J. Mater. Chem. A* **2017**, *5*, 3759–3773. [CrossRef]

51. Yang, Y.; Guo, Z.; Liu, W. Special Superwetting Materials from Bioinspired to Intelligent Surface for On-Demand Oil/Water Separation: A Comprehensive Review. *Small* **2022**, *18*, 2204624. [CrossRef] [PubMed]

52. Tie, L.; Li, J.; Liu, M.; Guo, Z.; Liang, Y.; Liu, W. Organic Media Superwettability: On-Demand Liquid Separation by Controlling Surface Chemistry. *ACS Appl. Mater. Interfaces* **2018**, *10*, 37634–37642. [CrossRef]

53. Gupta, R.K.; Dunderdale, G.J.; England, M.W.; Hozumi, A. Oil/Water Separation Techniques: A Review of Recent Progresses and Future Directions. *J. Mater. Chem. A* **2017**, *5*, 16025–16058. [CrossRef]

54. Zeng, X.; Yang, K.; Huang, C.; Yang, K.; Xu, S.; Wang, L.; Pi, P.; Wen, X. Novel pH-Responsive Smart Fabric: From Switchable Wettability to Controllable On-Demand Oil/Water Separation. *ACS Sustain. Chem. Eng.* **2019**, *7*, 368–376. [CrossRef]

55. Mao, X.; Wang, Y.; Yan, X.; Huang, Z.; Gao, Z.; Wang, Y.; Huang, L.; Kipper, M.J.; Tang, J. A Review of Superwetting Membranes and Nanofibers for Efficient Oil/Water Separation. *J. Mater. Sci.* **2023**, *58*, 3–33. [CrossRef]

56. Zheng, W.; Huang, J.; Li, S.; Ge, M.; Teng, L.; Chen, Z.; Lai, Y. Advanced Materials with Special Wettability toward Intelligent Oily Wastewater Remediation. *ACS Appl. Mater. Interfaces* **2021**, *13*, 67–87. [CrossRef]

57. Manouchehri, M. A Comprehensive Review on State-of-the-Art Antifouling Super(Wetting and Anti-Wetting) Membranes for Oily Wastewater Treatment. *Adv. Colloid Interface Sci.* **2024**, *323*, 103073. [CrossRef]

58. Yong, J.; Yang, Q.; Guo, C.; Chen, F.; Hou, X. A Review of Femtosecond Laser-Structured Superhydrophobic or Underwater Superoleophobic Porous Surfaces/Materials for Efficient Oil/Water Separation. *RSC Adv.* **2019**, *9*, 12470–12495. [CrossRef]

59. Qiu, L.; Sun, Y.; Guo, Z. Designing Novel Superwetting Surfaces for High-Efficiency Oil–Water Separation: Design Principles, Opportunities, Trends and Challenges. *J. Mater. Chem. A* **2020**, *8*, 16831–16853. [CrossRef]

60. Ma, W.; Samal, S.K.; Liu, Z.; Xiong, R.; De Smedt, S.C.; Bhushan, B.; Zhang, Q.; Huang, C. Dual pH- and Ammonia-Vapor-Responsive Electrospun Nanofibrous Membranes for Oil-Water Separations. *J. Membr. Sci.* **2017**, *537*, 128–139. [CrossRef]

61. Yong, J.; Chen, F.; Yang, Q.; Jiang, Z.; Hou, X. A Review of Femtosecond-Laser-Induced Underwater Superoleophobic Surfaces. *Adv. Mater. Interfaces* **2018**, *5*, 1701370. [CrossRef]

62. Su, B.; Tian, Y.; Jiang, L. Bioinspired Interfaces with Superwettability: From Materials to Chemistry. *J. Am. Chem. Soc.* **2016**, *138*, 1727–1748. [CrossRef] [PubMed]

63. Yong, J.; Chen, F.; Yang, Q.; Huo, J.; Hou, X. Superoleophobic Surfaces. *Chem. Soc. Rev.* **2017**, *46*, 4168–4217. [CrossRef] [PubMed]

64. Li, S.; Huang, L.; Wang, D.; Zhou, S.; Sun, X.; Zhao, R.; Wang, G.; Yao, T.; Zhao, K.; Chen, R. A Review of 3D Superhydrophilic Porous Materials for Oil/Water Separation. *Sep. Purif. Technol.* **2023**, *326*, 124847. [CrossRef]

65. Jung, Y.C.; Bhushan, B. Wetting Behavior of Water and Oil Droplets in Three-Phase Interfaces for Hydrophobicity/Philicity and Oleophobicity/Philicity. *Langmuir* **2009**, *25*, 14165–14173. [CrossRef] [PubMed]

66. Wenzel, R.N. Resistance of solid surfaces to wetting by water. *Ind. Eng. Chem.* **1936**, *28*, 988–994. [CrossRef]

67. Cassie, A.B.D.; Baxter, S. Large Contact Angles of Plant and Animal Surfaces. *Nature* **1945**, *155*, 21–22. [CrossRef]

68. Yong, J.; Chen, F.; Yang, Q.; Zhang, D.; Farooq, U.; Du, G.; Hou, X. Bioinspired Underwater Superoleophobic Surface with Ultralow Oil-Adhesion Achieved by Femtosecond Laser Microfabrication. *J. Mater. Chem. A* **2014**, *2*, 8790–8795. [CrossRef]

69. Cassie, A.B.D.; Baxter, S. Wettability of Porous Surfaces. *Trans. Faraday Soc.* **1944**, *40*, 546–551. [CrossRef]

70. Gao, H.; Liu, Y.; Wang, G.; Li, S.; Han, Z.; Ren, L. Switchable Wettability Surface with Chemical Stability and Antifouling Properties for Controllable Oil–Water Separation. *Langmuir* **2019**, *35*, 4498–4508. [CrossRef]

71. Popmintchev, T.; Chen, M.-C.; Popmintchev, D.; Arpin, P.; Brown, S.; Ališauskas, S.; Andriukaitis, G.; Balčiunas, T.; Mücke, O.D.; Pugzlys, A.; et al. Bright Coherent Ultrahigh Harmonics in the keV X-Ray Regime from Mid-Infrared Femtosecond Lasers. *Science* **2012**, *336*, 1287–1291. [CrossRef] [PubMed]

72. Vorobyev, A.Y.; Guo, C. Direct Femtosecond Laser Surface Nano/Microstructuring and Its Applications. *Laser Photonics Rev.* **2013**, *7*, 385–407. [CrossRef]

73. Bonse, J.; Krüger, J.; Höhm, S.; Rosenfeld, A. Femtosecond Laser-Induced Periodic Surface Structures. *J. Laser Appl.* **2012**, *24*, 042006. [CrossRef]

74. Chapman, H.N.; Spence, J.C.H. Femtosecond X-ray Protein Nanocrystallography. *Acta Crystallogr. A* **2010**, *66*, 9. [CrossRef]

75. Sugioka, K.; Cheng, Y. Ultrafast Lasers—Reliable Tools for Advanced Materials Processing. *Light Sci. Appl.* **2014**, *3*, e149. [CrossRef]

76. Anisimov, S.I.; Luk'yanchuk, B.S. Selected Problems of Laser Ablation Theory. *Phys. Uspekhi* **2002**, *45*, 293–324. [CrossRef]

77. Inogamov, N.A.; Zhakhovskii, V.V.; Ashitkov, S.I.; Petrov, Y.V.; Agranat, M.B.; Anisimov, S.I.; Nishihara, K.; Fortov, V.E. Nanospallation Induced by an Ultrashort Laser Pulse. *J. Exp. Theor. Phys.* **2008**, *107*, 1. [CrossRef]

78. Zhigilei, L.V. Dynamics of the Plume Formation and Parameters of the Ejected Clusters in Short-Pulse Laser Ablation. *Appl. Phys. A* **2003**, *76*, 339–350. [CrossRef]

79. Bulgakova, N.M.; Bourakov, I.M. Phase Explosion under Ultrashort Pulsed Laser Ablation: Modeling with Analysis of Metastable State of Melt. *Appl. Surf. Sci.* **2002**, *197–198*, 41–44. [CrossRef]

80. Leveugle, E.; Ivanov, D.S.; Zhigilei, L.V. Photomechanical Spallation of Molecular and Metal Targets: Molecular Dynamics Study. *Appl. Phys. A* **2004**, *79*, 1643–1655. [CrossRef]

81. Perez, D.; Lewis, L.J. Ablation of Solids under Femtosecond Laser Pulses. *Phys. Rev. Lett.* **2002**, *89*, 255504. [CrossRef] [PubMed]

82. Malinauskas, M.; Žukauskas, A.; Hasegawa, S.; Hayasaki, Y.; Mizeikis, V.; Buividas, R.; Juodkazis, S. Ultrafast Laser Processing of Materials: From Science to Industry. *Light Sci. Appl.* **2016**, *5*, e16133. [CrossRef] [PubMed]

83. Yan, H.; Abdul Rashid, M.R.B.; Khew, S.Y.; Li, F.; Hong, M. Wettability Transition of Laser Textured Brass Surfaces inside Different Mediums. *Appl. Surf. Sci.* **2018**, *427*, 369–375. [CrossRef]

84. Trdan, U.; Hočevar, M.; Gregorčič, P. Transition from Superhydrophilic to Superhydrophobic State of Laser Textured Stainless Steel Surface and Its Effect on Corrosion Resistance. *Corros. Sci.* **2017**, *123*, 21–26. [CrossRef]

85. Bai, X.; Yang, Q.; Fang, Y.; Zhang, J.; Yong, J.; Hou, X.; Chen, F. Superhydrophobicity-Memory Surfaces Prepared by a Femtosecond Laser. *Chem. Eng. J.* **2020**, *383*, 123143. [CrossRef]

86. Li, J.; Zhou, Y.; Wang, W.; Xu, C.; Ren, L. Superhydrophobic Copper Surface Textured by Laser for Delayed Icing Phenomenon. *Langmuir* **2020**, *36*, 1075–1082. [CrossRef]

87. Samanta, A.; Wang, Q.; Shaw, S.K.; Ding, H. Roles of Chemistry Modification for Laser Textured Metal Alloys to Achieve Extreme Surface Wetting Behaviors. *Mater. Des.* **2020**, *192*, 108744. [CrossRef]

88. Yong, J.; Chen, F.; Li, M.; Yang, Q.; Fang, Y.; Huo, J.; Hou, X. Remarkably Simple Achievement of Superhydrophobicity, Superhydrophilicity, Underwater Superoleophobicity, Underwater Superoleophilicity, Underwater Superaerophobicity, and Underwater Superaerophilicity on Femtosecond Laser Ablated PDMS Surfaces. *J. Mater. Chem. A* **2017**, *5*, 25249–25257. [CrossRef]

89. Yang, Z.; Tian, Y.L.; Yang, C.J.; Wang, F.J.; Liu, X.P. Modification of Wetting Property of Inconel 718 Surface by Nanosecond Laser Texturing. *Appl. Surf. Sci.* **2017**, *414*, 313–324. [CrossRef]

90. Bonse, J.; Gräf, S. Maxwell Meets Marangoni—A Review of Theories on Laser-Induced Periodic Surface Structures. *Laser Photonics Rev.* **2020**, *14*, 2000215. [CrossRef]

91. Ngo, C.-V.; Chun, D.-M. Fast Wettability Transition from Hydrophilic to Superhydrophobic Laser-Textured Stainless Steel Surfaces under Low-Temperature Annealing. *Appl. Surf. Sci.* **2017**, *409*, 232–240. [CrossRef]

92. Ma, Q.; Tong, Z.; Wang, W.; Dong, G. Fabricating Robust and Repairable Superhydrophobic Surface on Carbon Steel by Nanosecond Laser Texturing for Corrosion Protection. *Appl. Surf. Sci.* **2018**, *455*, 748–757. [CrossRef]

93. Sun, K.; Yang, H.; Xue, W.; He, A.; Zhu, D.; Liu, W.; Adeyemi, K.; Cao, Y. Anti-Biofouling Superhydrophobic Surface Fabricated by Picosecond Laser Texturing of Stainless Steel. *Appl. Surf. Sci.* **2018**, *436*, 263–267. [CrossRef]

94. Zhan, Y.L.; Ruan, M.; Li, W.; Li, H.; Hu, L.Y.; Ma, F.M.; Yu, Z.L.; Feng, W. Fabrication of Anisotropic PTFE Superhydrophobic Surfaces Using Laser Microprocessing and Their Self-Cleaning and Anti-Icing Behavior. *Colloids Surf. Physicochem. Eng. Asp.* **2017**, *535*, 8–15. [CrossRef]

95. Fang, Y.; Yong, J.; Chen, F.; Huo, J.; Yang, Q.; Zhang, J.; Hou, X. Bioinspired Fabrication of Bi/Tridirectionally Anisotropic Sliding Superhydrophobic PDMS Surfaces by Femtosecond Laser. *Adv. Mater. Interfaces* **2018**, *5*, 1701245. [CrossRef]

96. Song, Y.; Wang, C.; Dong, X.; Yin, K.; Zhang, F.; Xie, Z.; Chu, D.; Duan, J. Controllable Superhydrophobic Aluminum Surfaces with Tunable Adhesion Fabricated by Femtosecond Laser. *Opt. Laser Technol.* **2018**, *102*, 25–31. [CrossRef]

97. Yang, Z.; Liu, X.; Tian, Y. Insights into the Wettability Transition of Nanosecond Laser Ablated Surface under Ambient Air Exposure. *J. Colloid Interface Sci.* **2019**, *533*, 268–277. [CrossRef] [PubMed]

98. Wang, C.; Liu, B.; Luo, Z.; Ding, K.; Duan, J. Fabrication of Microholes Array on Titanium Foil by a Femtosecond Laser and a Surface's Wettability Switching. *Chin. Opt. Lett.* **2021**, *19*, 082201. [CrossRef]

99. Weber, F.R.; Kunz, C.; Gräf, S.; Rettenmayr, M.; Müller, F.A. Wettability Analysis of Water on Metal/Semiconductor Phases Selectively Structured with Femtosecond Laser-Induced Periodic Surface Structures. *Langmuir* **2019**, *35*, 14990–14998. [CrossRef] [PubMed]

100. Wood, M.J.; Servio, P.; Kietzig, A.-M. The Tuning of LIPSS Wettability during Laser Machining and through Post-Processing. *Nanomaterials* **2021**, *11*, 973. [CrossRef]

101. Chen, L.; Minakawa, A.; Mizutani, M.; Kuriyagawa, T. Study of Laser-Induced Periodic Surface Structures on Different Coatings Exhibit Super Hydrophilicity and Reduce Friction. *Precis. Eng.* **2022**, *78*, 215–232. [CrossRef]

102. Xing, Y.; Wu, Z.; Yang, J.; Wang, X.; Liu, L. LIPSS Combined with ALD MoS2 Nano-Coatings for Enhancing Surface Friction and Hydrophobic Performances. *Surf. Coat. Technol.* **2020**, *385*, 125396. [CrossRef]

103. Gnilitskyi, I.; Alnusirat, W.; Sorgato, M.; Orazi, L.; Lucchetta, G. Effects of Anisotropic and Isotropic LIPSS on Polymer Filling Flow and Wettability of Micro Injection Molded Parts. *Opt. Laser Technol.* **2023**, *158*, 108795. [CrossRef]

104. Gaudiuso, C.; Fanelli, F.; Mezzapesa, F.P.; Volpe, A.; Ancona, A. Tailoring the Wettability of Surface-Textured Copper Using Sub-THz Bursts of Femtosecond Laser Pulses. *Appl. Surf. Sci.* **2023**, *638*, 158032. [CrossRef]

105. Martínez-Calderon, M.; Rodríguez, A.; Dias-Ponte, A.; Morant-Miñana, M.C.; Gómez-Aranzadi, M.; Olaizola, S.M. Femtosecond Laser Fabrication of Highly Hydrophobic Stainless Steel Surface with Hierarchical Structures Fabricated by Combining Ordered Microstructures and LIPSS. *Appl. Surf. Sci.* **2016**, *374*, 81–89. [CrossRef]

106. Khan, S.A.; Ialyshev, V.; Kim, V.V.; Iqbal, M.; Al Harmi, H.; Boltaev, G.S.; Ganeev, R.A.; Alnaser, A.S. Expedited Transition in the Wettability Response of Metal Meshes Structured by Femtosecond Laser Pulses for Oil-Water Separation. *Front. Chem.* **2020**, *8*, 768. [CrossRef] [PubMed]

107. Dong, Z.; Sun, X.; Kong, D.; Chu, D.; Hu, Y.; Duan, J.-A. Spatial Light Modulated Femtosecond Laser Ablated Durable Superhydrophobic Copper Mesh for Oil-Water Separation and Self-Cleaning. *Surf. Coat. Technol.* **2020**, *402*, 126254. [CrossRef]

108. Yong, J.; Fang, Y.; Chen, F.; Huo, J.; Yang, Q.; Bian, H.; Du, G.; Hou, X. Femtosecond Laser Ablated Durable Superhydrophobic PTFE Films with Micro-through-Holes for Oil/Water Separation: Separating Oil from Water and Corrosive Solutions. *Appl. Surf. Sci.* **2016**, *389*, 1148–1155. [CrossRef]

109. Bakhtiari, N.; Azizian, S.; Mohazzab, B.F.; Jaleh, B. One-Step Fabrication of Brass Filter with Reversible Wettability by Nanosecond Fiber Laser Ablation for Highly Efficient Oil/Water Separation. *Sep. Purif. Technol.* **2021**, *259*, 118139. [CrossRef]

110. Qin, Z.; Xiang, H.; Liu, J.; Zeng, X. High-Performance Oil-Water Separation Polytetrafluoroethylene Membranes Prepared by Picosecond Laser Direct Ablation and Drilling. *Mater. Des.* **2019**, *184*, 108200. [CrossRef]

111. Ma, Z.; Lu, M.; Wang, W.; Hong, Z.; Chen, Z.; Zhang, W.; Pan, S.; Shui, L.; Zhang, C. Sucrose Solution Assisted Femtosecond Laser Ablation of Aluminum Film to Induce Nanospikes for Efficient and Stable Oil-Water Separation. *Surf. Coat. Technol.* **2021**, *417*, 127182. [CrossRef]

112. Ettel, D.; Havelka, O.; Isik, S.; Silvestri, D.; Wacławek, S.; Urbánek, M.; Padil, V.V.T.; Černík, M.; Yalcinkaya, F.; Torres-Mendieta, R. Laser-Synthesized Ag/TiO Nanoparticles to Integrate Catalytic Pollutant Degradation and Antifouling Enhancement in Nanofibrous Membranes for Oil–Water Separation. *Appl. Surf. Sci.* **2021**, *564*, 150471. [CrossRef]

113. Yu, P.; Lian, Z.; Xu, J.; Yu, Z.; Ren, W.; Yu, H. Fabrication of Superhydrophilic and Underwater Superoleophobic Metal Mesh by Laser Treatment and Its Application. *Mater. Res. Express* **2018**, *5*, 045013. [CrossRef]

114. Ahlawat, S.; Singh, A.; Mukhopadhyay, P.K.; Singh, R.; Bindra, K.S. Nanosecond Laser Induced Glass Particle Deposition over Steel Mesh for Long-Term Superhydrophilicity and Gravity Driven Oil Water Separation. *Mater. Chem. Phys.* **2021**, *263*, 124343. [CrossRef]

115. Li, B.; Lian, Z.; Yu, H.; Xu, J.; Shi, G.; Yu, Z.; Wang, Z. Underwater Superoleophobic Stainless Steel Mesh Fabricated by Laser Cladding a Copper Foil for Oil–Water Separation. *Mater. Res. Express* **2018**, *5*, 075014. [CrossRef]

116. Li, G.; Fan, H.; Ren, F.; Zhou, C.; Zhang, Z.; Xu, B.; Wu, S.; Hu, Y.; Zhu, W.; Li, J.; et al. Multifunctional Ultrathin Aluminum Foil: Oil/Water Separation and Particle Filtration. *J. Mater. Chem. A* **2016**, *4*, 18832–18840. [CrossRef]

117. Yong, J.; Yang, Q.; Hou, X.; Chen, F. Endowing Metal Surfaces with Underwater Superoleophobicity by Femtosecond Laser Processing for Oil-Water Separation Application. *Front. Phys.* **2020**, *8*, 305. [CrossRef]

118. Yu, H.; Lian, Z.; Xu, J.; Wan, Y.; Wang, Z.; Li, Y.; Yu, Z.; Weng, Z. Mechanically Durable Underwater Superoleophobic Surfaces Based on Hydrophilic Bulk Metals for Oil/Water Separation. *Appl. Surf. Sci.* **2018**, *437*, 400–409. [CrossRef]

119. Khew, S.Y.; Tan, C.F.; Yan, H.; Lin, S.; Thian, E.S.; Zhou, R.; Hong, M. Nanosecond Laser Ablation for Enhanced Adhesion of CuO Nanowires on Copper Substrate and Its Application for Oil-Water Separation. *Appl. Surf. Sci.* **2019**, *465*, 995–1002. [CrossRef]

120. Xia, L.; Chen, F.; Chao, J.; Zhang, D.; Tian, Y.; Zhang, D. Femtosecond Laser Engineered Eggshell Membrane for Durable Oil/Water Separation under Harsh Conditions. *J. Membr. Sci.* **2023**, *668*, 121242. [CrossRef]

121. Wang, J.; Xu, J.; Chen, G.; Lian, Z.; Yu, H. Reversible Wettability between Underwater Superoleophobicity and Superhydrophobicity of Stainless Steel Mesh for Efficient Oil–Water Separation. *ACS Omega* **2021**, *6*, 77–84. [CrossRef] [PubMed]

122. Zhou, Y.; Gu, X.; Yuan, Z.; Li, Y.; Wang, B.; Yan, J.; Zhao, D.; Liu, J.; Liu, X. PDMS Mesh with Reversible Super-Wettability for Oil/Water Separation. *Colloids Surf. Physicochem. Eng. Asp.* **2022**, *641*, 128462. [CrossRef]

123. Wang, J.; Xu, J.; Lian, Z.; Wang, J.; Chen, G.; Li, Y.; Yu, H. Facile and Green Fabrication of Robust Microstructured Stainless Steel Mesh for Efficient Oil/Water Separation via Waterjet-Assisted Laser Ablation. *Colloids Surf. Physicochem. Eng. Asp.* **2022**, *643*, 128703. [CrossRef]

124. Lian, Z.; Xu, J.; Wang, Z.; Yu, Z.; Weng, Z.; Yu, H. Nanosecond Laser-Induced Underwater Superoleophobic and Underoil Superhydrophobic Mesh for Oil/Water Separation. *Langmuir* **2018**, *34*, 2981–2988. [CrossRef] [PubMed]

125. Zhou, R.; Lin, S.; Shen, F.; Khew, S.Y.; Hong, M. A Universal Copper Mesh with On-Demand Wettability Fabricated by Pulsed Laser Ablation for Oil/Water Separation. *Surf. Coat. Technol.* **2018**, *348*, 73–80. [CrossRef]

126. Liu, Y.-Q.; Han, D.-D.; Jiao, Z.-Z.; Liu, Y.; Jiang, H.-B.; Wu, X.-H.; Ding, H.; Zhang, Y.-L.; Sun, H.-B. Laser-Structured Janus Wire Mesh for Efficient Oil–Water Separation. *Nanoscale* **2017**, *9*, 17933–17938. [CrossRef]